PROCEEDINGS, 48th Workshop on Geothermal Reservoir Engineering
Stanford University, Stanford, California, February 6-8, 2023
SGP-TR-224

The EGS Collab – Discoveries and Lessons from an Underground Experiment Series

Tim Kneafsey[1], Doug Blankenship[2], Jeff Burghardt[3], Tim Johnson[3], Pat Dobson[1], Paul C. Schwering[2], Chet Hopp[1], Mark White[3], Joseph P. Morris[4], Chris Strickland[3], Vince Vermuel[3], Pengcheng Fu[4], Mathew Ingraham[2], William Roggenthen[5], Thomas Doe[6], Jonathan B. Ajo-Franklin[7], Lianjie Huang[8], Verónica Rodríguez Tribaldos[1], Yves Guglielmi[1], Hunter Knox[3], Paul Cook[1], Florian Soom[1], Craig Ulrich[1], Luke Frash[8], Ghanashyam Neupane[9], Tatiana Pyatina[10], Jon Weers[11], Earl Mattson[12], Michelle Robertson[1], and The EGS Collab Team*

[1]Lawrence Berkeley National Laboratory, Berkeley, California, USA, [2]Sandia National Laboratories, Albuquerque, New Mexico, USA, [3]Pacific Northwest National Laboratory, Richland, Washington, USA, [4]Lawrence Livermore National Laboratory, Livermore, California, USA, [5]South Dakota School of Mines & Technology, Rapid City, South Dakota, USA, [6]Doe Geo, Redmond, Washington, USA, [7]Rice University, Houston, Texas, USA, [8]Los Alamos National Laboratory, Los Alamos, New Mexico, USA, [9]Idaho National Laboratory, Idaho Falls, Idaho, USA, [10]Brookhaven National Laboratory, Upton, New York, USA, [11]National Renewable Energy Laboratory, Golden, Colorado, USA, [12]Mattson Hydrology LLC, Victor, Idaho, USA

tjkneafsey@lbl.gov

Keywords: Enhanced Geothermal Systems, EGS Collab, stimulation, crystalline rock, Sanford Underground Research Facility, coupled process modeling, experimental, field test, flow test, multi-physics monitoring

ABSTRACT

The EGS Collab project performed densely-monitored rock stimulation and flow tests at the 10-m scale in the Sanford Underground Research Facility (SURF) in Lead, South Dakota to inform challenges in implementing enhanced geothermal systems (EGS). This project, supported by the US Department of Energy, gathered data and observations from the field tests to understand processes and to build confidence in numerical modeling of the processes. The project was organized into three sets of field experiments. Experiment 1 examined hydraulic fracturing at a depth of approximately 1.5 km in a well-characterized phyllite. Geophysical monitoring instrumentation installed in six of eight sub-horizontal boreholes was used to monitor stimulation events and flow tests. The other two boreholes were used to perform and carefully measure water injection and production. More than a dozen stimulations and nearly one year of flow tests were performed. The stimulation and dynamic flow tests allowed for the collection and analysis of detailed observations of processes. Flow tests of ambient temperature and chilled water injections were performed with intermittent tracer tests to examine system behavior. We achieved adaptive control of the tests using close monitoring of rapidly disseminated data and near-real-time simulation. Numerical simulation was critical in answering key experimental design questions, forecasting fracture behavior, and analyzing results. We were successful in performing many simulations in near-real-time in conjunction with the field experiments, with more detailed simulations performed later.

Experiment 2 examined hydraulic shearing in an amphibolite test bed at SURF at a depth of about 1.25 km with stress and fracture conditions that are different from Experiment 1. Approximately five fracture set orientations were encountered and the testbed was designed accordingly to maximize the likelihood of shear stimulation. The testbed, designed for primarily remote operation, consisted of nine boreholes, in addition to two earlier-drilled characterization boreholes. Four boreholes contained grouted-in geophysical instruments, and the other five open boreholes were adaptively used for injection, production, and geophysical monitoring. Experiment 3 was performed in the same test bed as Experiment 2 and consisted of investigating various stimulation strategies, ultimately resulting in connecting the injection and production boreholes with hydraulic fractures. After creating a flow-through system, ambient-temperature and chilled water flow tests were performed with intermittent tracer tests to help understand flow and heat transfer in the system. Numerical simulations

---

*J. Ajo-Franklin, T. Artz, T. Baumgartner, K. Beckers, G. Bettin, D. Blankenship, A. Bonneville, L. Boyd, S. Brown, J.A. Burghardt, C. Chai, A. Chakravarty, T. Chen, Y. Chen, B. Chi, K. Condon, P.J. Cook, D. Crandall, N. Creasy, R. DeBoer, P.F. Dobson, T. Doe, C.A. Doughty, D. Elsworth, J. Feldman, Z. Feng, A. Foris, L.P. Frash, Z. Frone, P. Fu, K. Gao, A. Ghassemi, Y. Guglielmi, B. Haimson, A. Hawkins, J. Heise, C. Hopp, M. Horn, R.N. Horne, J. Horner, M. Hu, H. Huang, L. Huang, K.J. Im, M. Ingraham, E. Jafarov, R.S. Jayne, T.C. Johnson, S.E. Johnson, B. Johnston, S. Karra, K. Kim, D.K. King, T. Kneafsey, H. Knox, J. Knox, D. Kumar, K. Kutun, M. Lee, D. Li, J. Li, K. Li, Z. Li, M. Maceira, P. Mackey, N. Makedonska, C.J. Marone, E. Mattson, M.W. McClure, J. McLennan, T. McLing, C. Medler, R.J. Mellors, E. Metcalfe, J. Miskimins, J. Moore, C.E. Morency, J.P. Morris, T. Myers, S. Nakagawa, G. Neupane, G. Newman, A. Nieto, T. Paronish, R Pawar, P. Petrov, B. Pietzyk, R. Podgorney, Y. Polsky, J. Pope, S. Porse, J.C. Primo, T. Pyatina, J. Quintanar, C. Reimers, B.Q. Roberts, M. Robertson, V. Rodríguez-Tribaldos, W. Roggenthen, J. Rutqvist, D. Rynders, M. Schoenball, P. Schwering, V. Sesetty, C.S. Sherman, A. Singh, D. Sirota, M.M. Smith, H. Sone, E.L. Sonnenthal, F.A. Soom, D.P. Sprinkle, S. Sprinkle, J. St. Clair, C.E. Strickland, J. Su, Y. Tanaka, N. Taverna, D. Templeton, J.N. Thomle, C. Ulrich, N. Uzunlar, A. Vachaparampil, C.A. Valladao, W. Vandermeer, G. Vandine, D. Vardiman, V.R. Vermeul, J.L. Wagoner, H.F. Wang, J. Weers, N. Welch, J. White, M.D. White, P. Winterfeld, T. Wood, S. Workman, H. Wu, Y.S. Wu, E.C. Yildirim, Y. Zhang, Y.Q. Zhang, Q. Zhou, M.D. Zoback

were used to design each of the experiments and in turn were validated using the comprehensive monitoring datasets that were collected during each of the field experiments.

1. INTRODUCTION

Enhanced or engineered geothermal systems (EGS) offer tremendous potential as an energy resource supporting the energy security of the United States, and implementation is being examined worldwide. Estimates exceed 500 GWe for the western US, surpassing the resource base hosted by conventional hydrothermal systems (Williams et al., 2008), and up to an order of magnitude larger including the entire United States (Augustine, 2016). Implementation of an EGS will typically require stimulation to generate appropriate in-situ conditions allowing communication among multiple wells. Techniques to perform these stimulations require greater understanding for implementation. Additional improvements needed for implementing EGS include improving imaging and monitoring techniques for permeability enhancement and evolution, understanding and managing associated seismicity, improving technologies for zonal isolation for multistage stimulations under elevated temperatures, developing technologies to isolate zones for controlling fast flow paths within the reservoir to reduce early thermal breakthrough, and developing scientifically-based long-term EGS reservoir sustainability and management techniques.

The approach of the EGS Collab project was to refine our understanding of rock mass response to stimulation using accessible deep rock. We performed 10-m spatial scale experiments under stresses relevant to EGS (at 1.25 and 1.5 km depth) in crystalline rock. Our tests and analyses were performed to support validation of thermal-hydrological-mechanical-chemical (THMC) modeling approaches. In addition, the EGS Collab project tested and improved novel and conventional field monitoring tools. By observing system behavior during our experiments, we gained insight into permeability enhancement and evolution in crystalline rock. These observations and interpretations provide understanding of creating sustained and distributed permeability for heat extraction in an EGS reservoir by generating new fractures that complement existing fractures.

The project consisted of three multi-test experiments to increase understanding of 1) hydraulic fracturing (Experiment 1 E1), 2) shear stimulation (Experiment 2 – E2), and 3) other stimulation methods in Experiment 3 (E3). Modeling supported experiment design and observation interpretation. Post-test modeling and analysis were performed to examine the effectiveness of our modeling and monitoring tools and approaches. This is to allow building confidence in and improving the array of modeling and monitoring tools and approaches.

The EGS Collab experiments were conducted at the Sanford Underground Research Facility (SURF) in Lead, South Dakota (Heise, 2015). SURF maintains and upgrades underground facilities at multiple depths in a variety of rock types remaining from the former Homestake gold mine for scientific investigation. SURF hosts a number of scientific projects ranging from collection and analysis of rock and water samples for biological investigation, to enormous infrastructure-intense multibillion dollar physics experiments. EGS Collab E1 was performed at 1.5 km depth (the 4850-foot depth level) as shown in Figure 1. E1 tests established a fracture network using hydraulic fracturing that connects an injection well and a production well (Kneafsey et al., 2021a; Kneafsey et al., 2021b; Kneafsey et al., 2021c; Morris et al., 2018). More than a dozen stimulations were performed and the injection and production boreholes were connected (White et al., 2019). Flow tests using initially ambient-temperature water and then chilled water (as an analog to EGS) were conducted over the course of a year (Kneafsey et al., 2021b), and tracer tests were intermittently performed to understand flow conditions (Mattson et al., 2019a; Mattson et al., 2019b; Neupane et al., 2020; Wu et al., 2019a; Wu et al., 2019b). Details of E1 have been extensively covered in previous publications[†] and we refer the reader to these works.

E2 was intended to investigate shear stimulation. The testbed for this experiment is at 1.25 km depth (4100-foot depth) (Figure 1). This testbed is in the Yates amphibolite (a blocky, low permeability rock) with subsurface stress conditions different from those of E1 (Ingraham et al., 2020). Based on information available at the time, several sets of analyses showed a reasonable probability of shearing if a sufficiently weak fracture with an appropriate orientation relative to the stress field were intercepted at the site (Burghardt et al., 2020; Dobson et al., 2018; Singh et al., 2019). Fractures and features observed at the drift wall were mapped, and a 10 m horizontal borehole (TH4100) and a 50 m vertical borehole (TV4100) were drilled. TV4100 penetrated an unexpected ~10m thick rhyolite layer within the amphibolite that is likely to be continuous and present beneath our test bed. Eighteen stress tests were performed in TV4100, eight of which used the Step-Rate Injection Method for Fracture In-Situ Properties (SIMFIP) tool (Guglielmi et al., 2015; Guglielmi et al., 2021a; Guglielmi et al., 2021b; Guglielmi et al., 2014) to quantify three-dimensional displacement during testing. These stress tests showed significant stress heterogeneity and lower than expected stress anisotropy (Ingraham et al., 2020). Instantaneous shut-in pressures (ISIP – providing an estimate of minimum principal stress) in the deeper amphibolite below the thick rhyolite layer were ~ 27.6 MPa (4000 psi), ~ 18.6 MPa (2700 psi) in the rhyolite, and ~ 21.4 MPa (3100 psi) in the upper amphibolite (Kneafsey et al., 2021b). A sleeve fracture reopening test conducted above the rhyolite layer, together with the absence of borehole breakouts suggests that the most probable magnitude of the intermediate principal stress, which is subhorizontal, is between 30 and 40 MPa (Burghardt et al., 2022). Since the lithostatic stress at the site is approximately 35 MPa, this places the stress state as transitional between a normal faulting and strike-slip regime. Because of the low stress in the rhyolite and the complexity that it introduced, the E2 test bed is designed to be entirely *above* the rhyolite layer. More detailed descriptions of the geology, testbed characterization, and evaluation of stresses are contained in Kneafsey et al. (2022b).

[†] https://scholar.google.com/citations?hl=en&user=h-rd4hkAAAAJ&view_op=list_works&authuser=1&sortby=pubdate

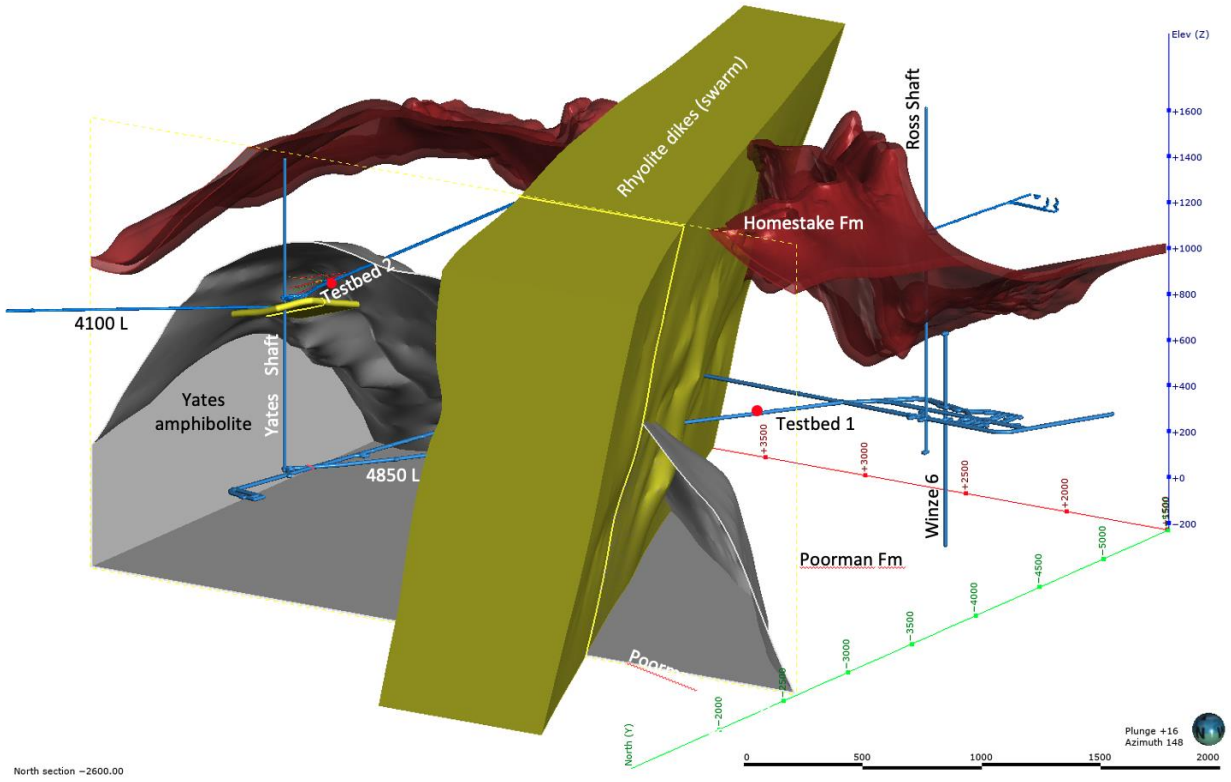

Figure 1. Geologic model showing locations of the EGS Collab Testbed 1 (on 4850 L) and Testbed 2 (on 4100 L). Testbed 1 was developed entirely within a carbonate-mica phyllite of the upper Poorman Formation. Testbed 2 was developed within the amphibolite sequences of the Yates Member of the Poorman Formation.

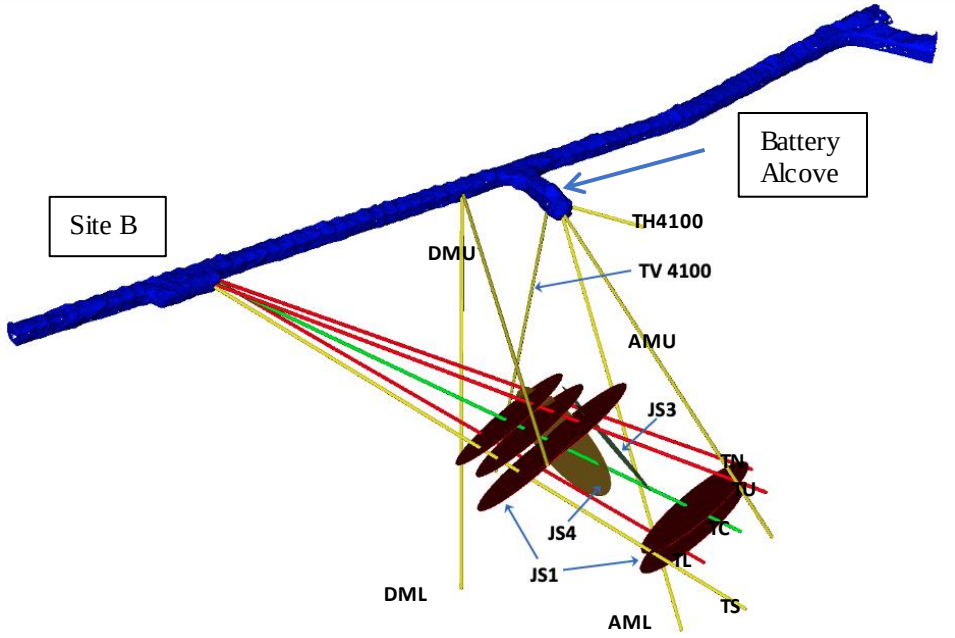

Figure 2. Borehole orientations for Experiment 2, oblique view. The thick blue object represents the drift (mine tunnel), the green line represents the injection well, red lines represent production wells, and yellow lines represent monitoring wells. Other than the vertical well TV4100, all wells are subhorizontal. Disks indicate natural fracture orientations that connect the injection and production wells and hotter colors indicate greater slip tendency. JS1 has a higher slip tendency than other fracture set orientations.

2. EXPERIMENTS 2 AND 3 TESTBED

A detailed description of the E2 testbed is presented in Kneafsey et al. (2022c). Briefly however, nine ~10 cm diameter subhorizontal boreholes from 55 to 80 m deep were drilled for this experiment (Figure 2). Two pairs of monitoring wells containing grouted sensors fan out from a location in the Battery Alcove (AMU and AML) and a location in the drift (DMU and DML). An injection well (TC) surrounded by four open injection/production/monitoring wells (TU, TL, TN, TS) extend from Site B. Five joint sets identified in the testbed were considered in the analyses of hydraulic shearing (Burghardt et al., 2022). Well TC was oriented to optimally intersect fractures that were interpreted to be best oriented for shear stimulation while also avoiding the sub-horizontal rhyolite zone below the drift (Kneafsey et al., 2022c).

Instrumentation for the experiment includes active seismic sources and sensors for Continuous Active Source Seismic Monitoring (CASSM) and passive seismic monitoring, a hybrid fiber-optic cable with single mode (strain – DSS, acoustic – DAS) and multi-mode fiber (temperature – DTS,), electrical resistivity tomography (ERT), and thermistors. These were deployed and grouted in AMU, AML, DMU, and DML (Figure 3). CASSM sources, an array of hydrophones, ERT electrodes and multi-mode fiber-optic cable for DTS were also deployed in TS. ERT and multi-mode fiber were deployed in TU, TL, and TN as allowed by experiment constraints. A new Downhole Robotic Stress Analysis (DORSA) tool measuring borehole displacement in six degrees of freedom was also constructed and co-deployed with ERT sensors in well TN (Figure 3). Stimulations could be performed in any of the wells emanating from Site B, with initial stimulations targeted for the central borehole TC. Initial stimulations used the SIMFIP tool to quantify multidirectional strain during stimulation, and subsequent stimulations were performed with other straddle packer sets.

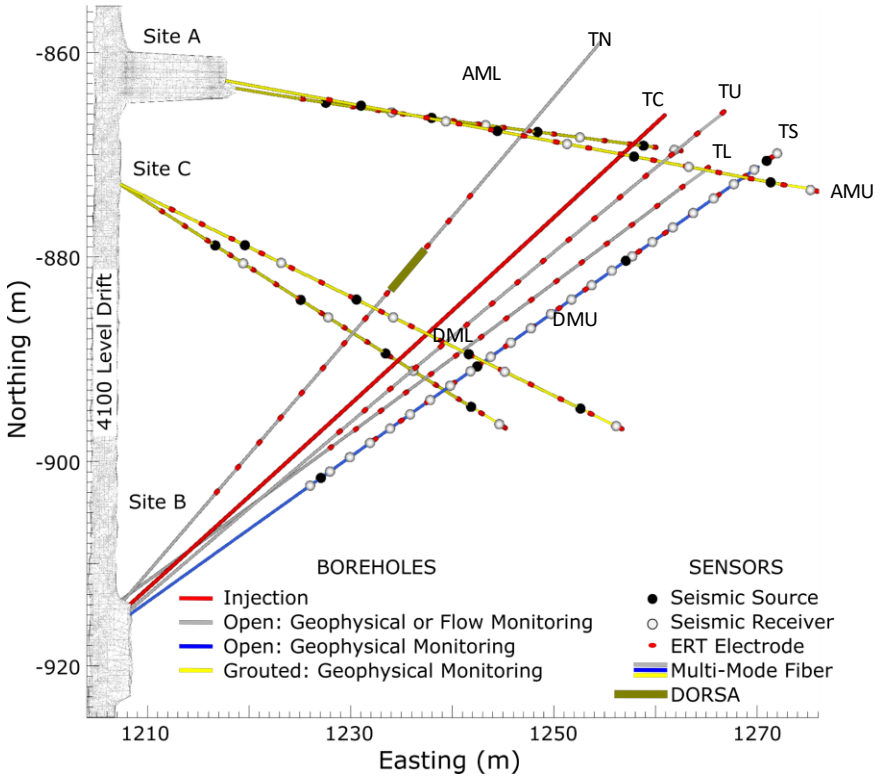

Figure 3. Plan view of geophysical monitoring borehole layout and sensor locations for E2. Coordinates are based on the Homestake coordinate grid system.

2.1 Testbed 2 stress conditions

Initial calculations were promising with respect to shearing some fractures in the rock (Singh et al., 2019), however later calculations based on more complete information indicated that the rock was less likely to shear, as maximum shear-to-normal stress ratios were about 0.35, which is significantly less than the desired value of 0.6 (Figure 4, and Figure 5) (Burghardt et al., 2022). Meng et al. (2021b) and Meng et al. (2022) conducted a series of laboratory tests on actual core samples from the 4100 level, and found that most of the tested sealed fractures did not fail at in-situ shear conditions. Additionally, for shear stimulation, the selected fracture set would need to be in pressure communication with the well and able to take water at a rate adequate pressurize a significant area of the fracture within the time-frame of the stimulation, which did not occur.

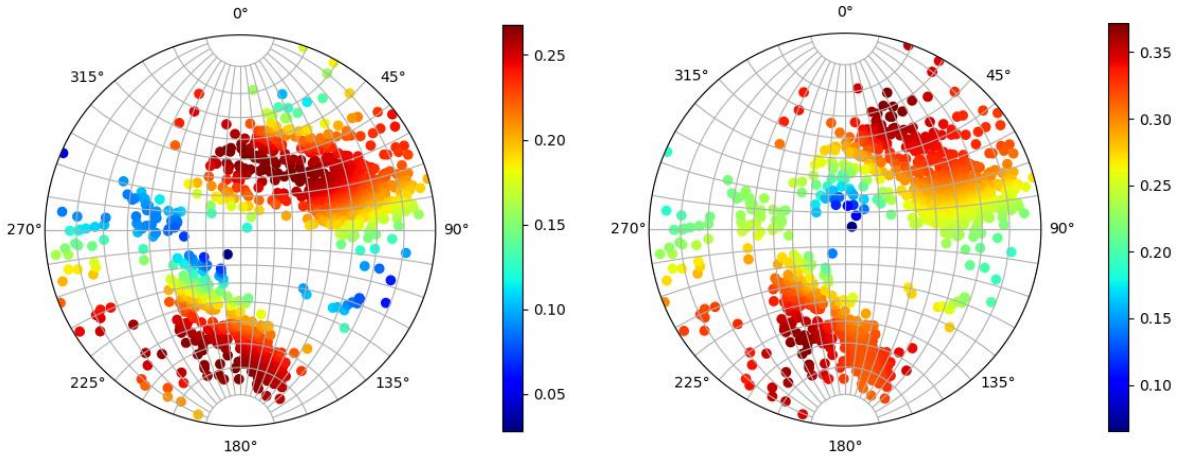

Figure 4. Left - Equal angle lower hemisphere projection of poles of identified fractures in E2-TC, colored according to the mean shear-to-normal stress ratio under the hypothesis that the principal stresses are rotated from vertical/horizontal. Right - Equal angle lower hemisphere projection of poles of identified fractures in E2-TC under the assumption that the principal stresses are vertical/horizontal. Both plots are colored according to the mean critical shear-to-normal stress ratio (i.e., maximum friction coefficient that permits slip with zero cohesion).

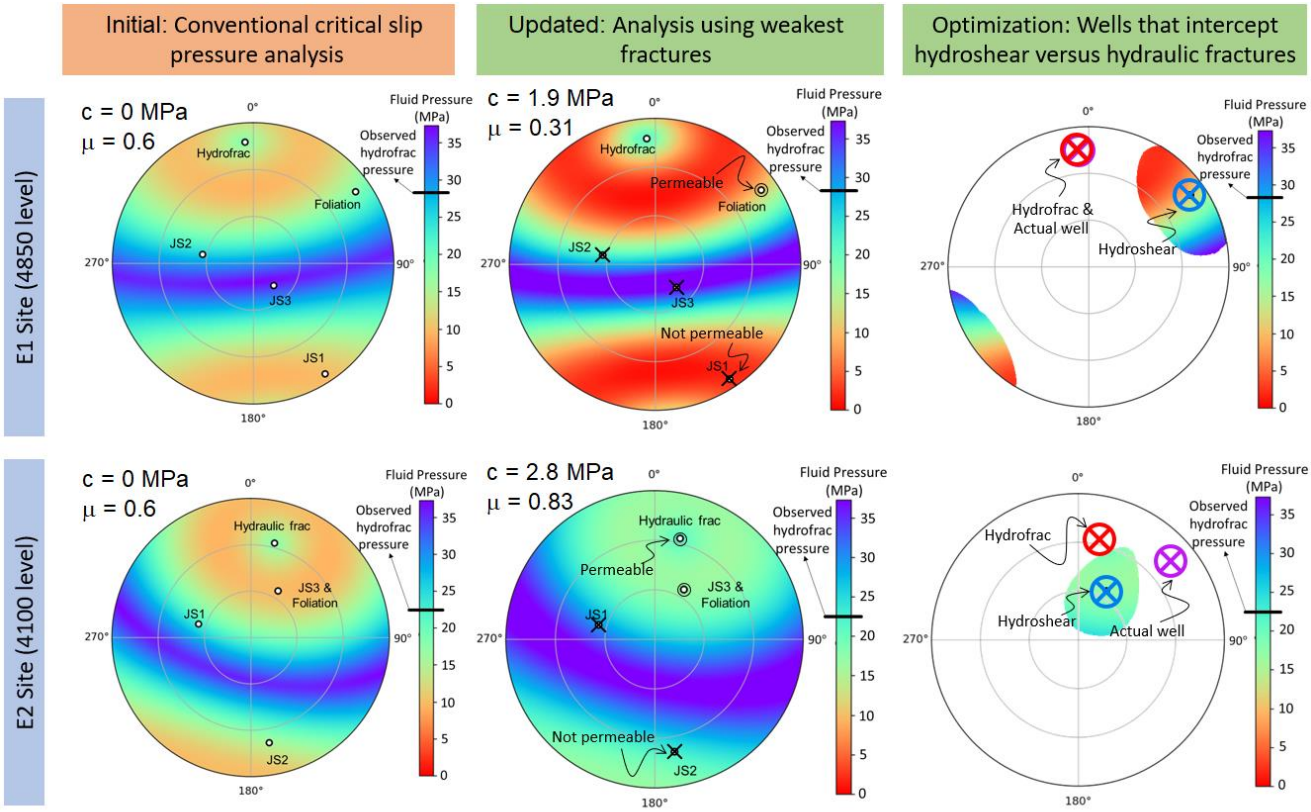

Figure 5. Geomechanical analysis informed by in-situ stress tests (Ingraham et al., 2020; Burghardt et al, 2022), borehole fracture mapping (Ulrich et al., 2018), and laboratory tests (Meng et al., 2021a; Meng et al., 2022), showing the initially expected and updated shear slip predictions at the E1 and E2 sites as a function of fracture orientation and critical slip pressure.

Using the updated in-situ stress and fracture data from the exploratory boreholes (TH4100 and TV4100), an ensemble of 16,000 simple discrete fracture network stimulation, circulation, and heat recovery models were completed (Frash et al., 2022) using LANL's open-source Geothermal Design Tool (GeoDT) (Frash, 2021, 2022). The key outputs from this modeling effort include: 1. at injection at rates slower than 2 L/min, the fracture system could be diffusion dominated with flow distributed through the fracture network into the drift

and various monitoring wells. 2. At higher injection rates the relative proportion of flow into the production wells would favor TN, TL, TU, TS, other intervals of TC, and then other locations, in order from highest to lowest production rate. 3. At injection rates faster than 40 L/min, the model predicts that the production wells would be overwhelmed and flow would predominantly occur from the mine drift. The circulation rate recommendations using GeoDT indicated an optimal range of 3 to 22 L/min (See below), estimated with the goal of achieving at least 10% thermal drawdown in the fastest flowing production well within six months (Frash et al., 2022). Flow rates exceeding 5 L/min were not applied during the test because of observed water breakthrough to the drift.

3. THERMAL MODELING

3.1 Initial Temperature Field

Experiments 1 and 2 were both conducted in rock volumes adjacent to a mine drift. These drifts were excavated during the mining activities of the Homestake Gold Mine, which began in the late 1870s and continued until 2001. Mining operations involved both dewatering and active ventilation, and the dewatering activities continued until June 10, 2003. At this point water levels rose from below the 8000 Level (2450 m bgs), reaching the 4850 Level (1500 m bgs) around September 2007. Dewatering and ventilation activities resumed with the transition from mining operations to scientific research, and the 4850 Level (1500 m bgs) was reopened for access on May 13, 2009. A numerical model of the temperature field within the rock volume of E1 was developed and compared against temperature logs taken in a series of vertical kISMET boreholes (Oldenburg et al., 2020; Roggenthen & King, 2017). These simulations required the consideration of cooling of the drift walls via ventilation to accurately match the temperature logs. The resulting temperature field within rock volume of E1, a combination of radial cooling around the drift and the geothermal gradient, and the decreasing temperature gradient toward the drift, yielded a similar gradient in mechanical stress, which influenced the direction of fracture propagation during the stimulation stages of E1. It was anticipated that ventilation through the drift adjacent to the rock volume of E2 would have a similar impact on the temperature field. As this temperature field serves as the initial conditions for the chilled water test, an accurate accounting of this is was important. As with E1 (White et al., 2018), a series of numerical simulations were conducted and compared against DTS data from the monitoring boreholes (i.e., AMU, AML, DMU, and DML). As the battery alcove extends into the experimental volume, a 3-dimensional computational grid was used to model the temperature field. As with the simulations on the 4850 Level, the principal unknown was the thermal conductivity of the rock. A homogeneous rock thermal conductivity distribution was assumed for the simulations for both experiments. The computational domain is shown in Fig. 20, with the drift being considered as inactive grid cells allowing boundary conditions to be imposed on the drift walls. For an accurate match with the DTS records, it was necessary to impose a constant temperature on the main drift walls and a temperature gradient on the battery alcove walls, increasing in temperature with depth into the alcove. A rock thermal conductivity of 5.0 W/m K was determined to yield the best agreement with the kISMET borehole temperature logs in the graphite-rich phyllite rock of the E1 testbed (similar to reported Poorman measurements by Blackwell (1967); Clark (1966)), which range from 3.3 to 4.9 W/m K), and a conductivity of 3.8 W/m K was found to provide good agreement with the DTS measurements in E2, as shown in Figure 6 right. Blackwell (1967); Clark (1966) report thermal conductivity values for the Yates amphibolite ranges from 2.5 to 3.8 W/m K.

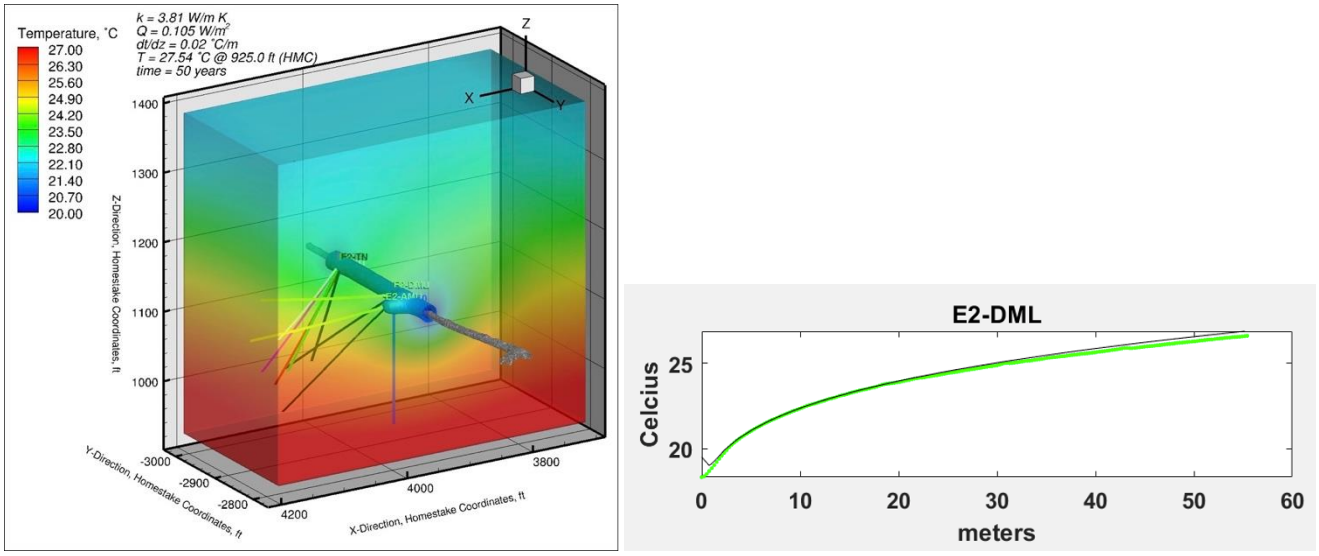

Figure 6. Numerical simulations with STOMP-GT of the temperature field with the E2 testbed, prior to the chilled-water circulation test.

3.2 Thermal Breakthrough Prediction

Thermal breakthrough predictions were completed to estimate the required injection rate that should induce at least a 10% decline in produced water temperature during the circulation test estimated to be six months. However, we anticipated that faster breakthroughs would be beneficial for model validation, if safely attainable. Thermal breakthrough modeling was completed using: 1) Gringarten theory for heat extraction from rock, 2) STOMP-GT, and 3) GeoDT. All three analyses predicted similar required injection rates in the range of 3 to 20 L/min to induce a 10% (or greater) reduction in the produced fluid temperature. The ideal flow rate depended on the distribution

of flow within the site where fast flow to a single production well could achieve thermal breakthrough more rapidly at a constant injection rate than flow through a more diffuse fracture network. Key sources of uncertainty that were identified by this modeling effort included unknown fracture heterogeneity, unknown flowing fracture network geometry, and uncertainty regarding the thermal conductivity of the matrix rock. Of these, the unknown fracture geometry, and hence unknown heat transfer area, was the most significant and least constrained parameter with respect to predicting thermal drawdown behavior.

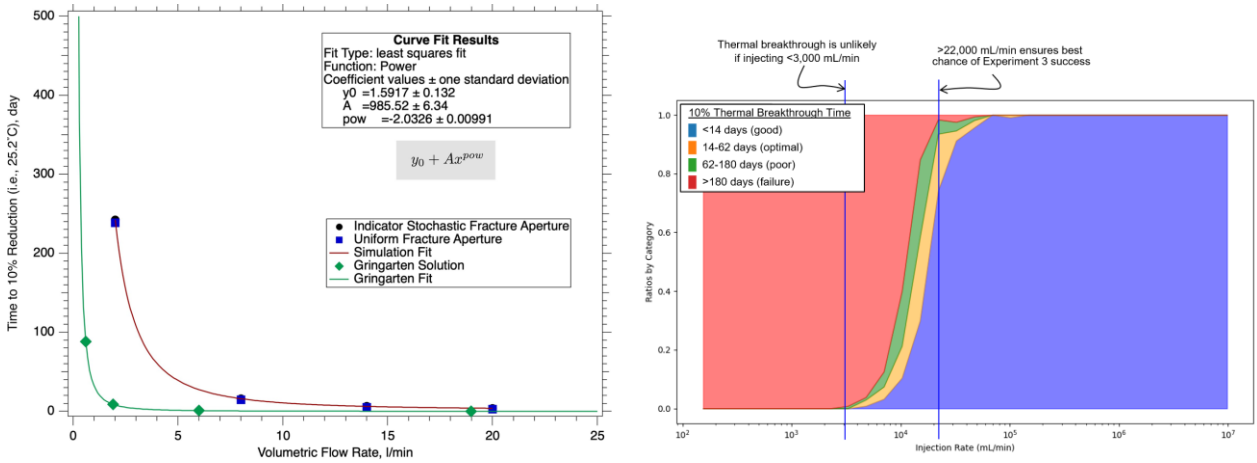

Figure 7. Left Thermal decline predictive analysis with fracture permeability heterogeneity completed using STOMP-GT and the Gringarten Solution. Predicted minimum nominal flow rate to achieve thermal breakthrough within 6 months was 3 L/min injection rate. Right – Predicted minimum injection rate for thermal breakthrough as a function of injection rate into borehole TC. This plot shows results using GeoDT to account for uncertainty in the fracture geometry, flow paths, and thermal conductivity. Faster flow rates are preferable to ensure that breakthrough is observed within the expected 6 months duration of the experiment (Frash et al., 2022).

4. EXPERIMENT 2 – SHEAR STIMULATION

The E2 stimulation consisted of identifying the fracture most likely to shear and pressurizing it to at most 90% of the estimated minimum principal stress. These conditions would maximize the possibility of shearing while precluding hydraulic fracturing. The SIMFIP was placed with packers straddling this highest slip probability fracture (referred to as Zone 7, at depths of 192.4-200.3 ft), and the zone was pressurized to 2340 psi (approximately 90% of the minimum principal stress) for two weeks. Over the two weeks, the rock and fractures did not uptake a significant quantity of water (only tens of mL/day) which would be needed to induce shear. This result indicates that hydraulic shearing as a mechanism for fracture stimulation was unsuccessful in E2. Based on our experience, we can expect similar, but amplified difficulties when planning hydraulic shear stimulation at field sites where much less data are available. This attempt may have been complicated by the observation that nearly all of the fractures in the E2 testbed were mineralized. The mineralization resulted in fracture cementation inhibiting flow into the fracture and strengthening the fractures, limiting hydraulic reactivation.

5. EXPERIMENT 3 –STIMULATION AND FLOW

Following the attempt at shear stimulation at pressures below the minimum principal stress, additional stimulations were conducted where the pressure was permitted to exceed the minimum principal stress (Experiment 3 - E3). The stimulations were performed in three intervals in well TC working from the bottom of the hole upwards: 192.4 – 200.3 ft (Zone 7), 168.7-176.6 ft (Zone 4), and 145.0-152.9 ft (Zone 1) (Figure 8). The Zone 7 stimulation was performed at low flow rates ramping up from 3 mL/min to 400 mL/min with a total injected volume of 300 L. The Zone 4 stimulation was performed by cycling the pressure about the minimum principal stress (40 L total volume). The Zone 1 stimulation was performed by breaking the rock down at 1 L/min and extending the fracture at 5 L/min with a total injected volume of about 400 L. These stimulations (Table 1) are described in Kneafsey et al. (2022a) and selected observations from these stimulations are presented below.

Table 1. Experiment 3 stimulations.

Zone, Interval	*Method*	*Volume*	*Connects to/Interferences*	*Dates*	*Breakdown (psi)*
TC Zone 7 *192.4-200.3 ft*	*Increasing flow from 0.003 L/min to 0.4 L/min*	*300 L*	*TN, TS (dripping), AMU*	*4/11/22-4/12/22*	*3650*
TC Zone 4 *168.7-176.6 ft*	*Cyclic (2800 < P < 4500 psi)*	*40 L*	*TN, TL, and TS (a little)*	*4/14/22*	*Not clear*

TC Zone 1 ***145.0-152.9 ft***	***1 L/min, 5 L/min***	***400 L***	***TN, TL, TS, and TV4100***	***4/13/22***	***~3400 psi***
TU Zone 3 ***177.4-179.6 ft***	***1 L/min, 5 L/min***	***1200 L***	***TC, TN, and TL***	***5/5/22-5/7/22***	***5500 psi***
TC Zone 4 ***165.5-167.7 ft***	***2 L/min***			***5/19/22***	
TU Zone 3 ***177.4-179.6 ft***				***5/19/22***	***Set up flow test***

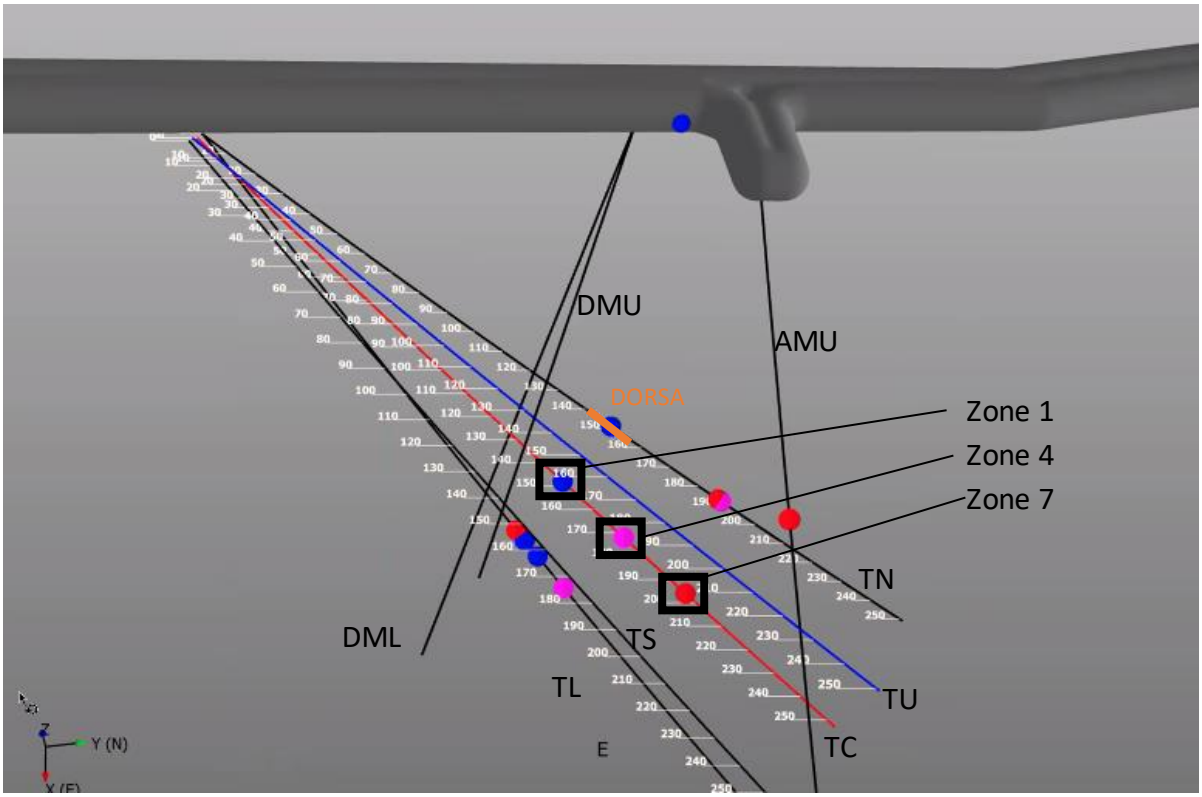

Figure 8. Stimulation locations in TC and early fracture intersections indicated by colored dots. Red - Zone 7, pink - Zone 4, blue - Zone 1.

5.1 Stimulation 1 – TC Zone 7 – Slow Flow

The SIMFIP tool was left at the location in TC where it had held a pressure just below the minimum principal stress for Experiment 2. This stimulation initiated by pumping water at 3 mL/min into the packed interval on April 11, 2022 at around 17:00 UTC. Following breakdown, the rate was stepwise increased each ~80 minutes or more until a maximum flow rate of 400 mL/min was reached (Figure 9). The rationale for this approach was to propagate the fracture with as low of a flow rate as was practically possible so as to maximize the potential for activation of natural fractures. After several hours of pumping at 400 mL/min, breakthrough into the production wells (primarily TN with a drip observed from TS) was observed. Flows as high as 250 mL/min were recovered from TN (63% of the inflow rate). An elevated temperature spike in the DTS data in well AMU indicated that the stimulation intersected with well AMU at ~ 5:23 UTC on April 12 (Figure 10). Spikes in strain can also be observed in some of the DAS monitoring systems at the same time and location, however changes in strain around that zone in AMU began at least 6 hours prior to breakthrough (Figure 11). The initial strain signal was somewhat diffuse with a larger zone, just below the location of the fracture, showing compressive strain. The breakthrough is evidenced by a more defined extensional signal (Figure 11 center). A slow drip of water from the AMU wellhead was also observed. The ERT data are consistent with the strain and temperature data (Figure 12). This figure shows a decrease in conductivity near the injection site. This decrease is likely caused by pressure in the packers squeezing water out of pores by the increased compressive stress adjacent to the borehole and fracture (Johnson et al., 2021). A decrease in conductivity is also observed near the breakthrough location in AMU. This

may also be caused by compression of the rock as shown by the DAS strain data prior to breakthrough. Additionally, water in well AMU increased conductivity and that is clearly observed in Figure 12. When it was determined that the fracture intersected the monitoring well, the injection was stopped, and outflows from production wells and E2-AMU decreased slowly with time.

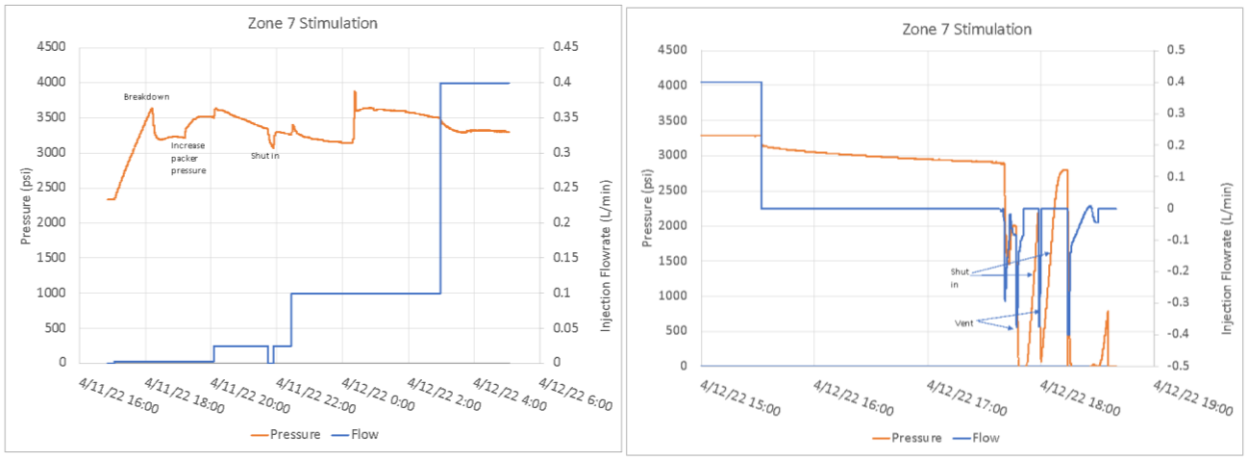

Figure 9. Pressure and flow for Stimulation 1 at Zone 7. Left, breakdown and initial fracture extension. Note: breakdown occurred with an injection flow rate of 3 mL/min. Right, continued extension, shut in, and alternating episodes of shut-in and well venting.

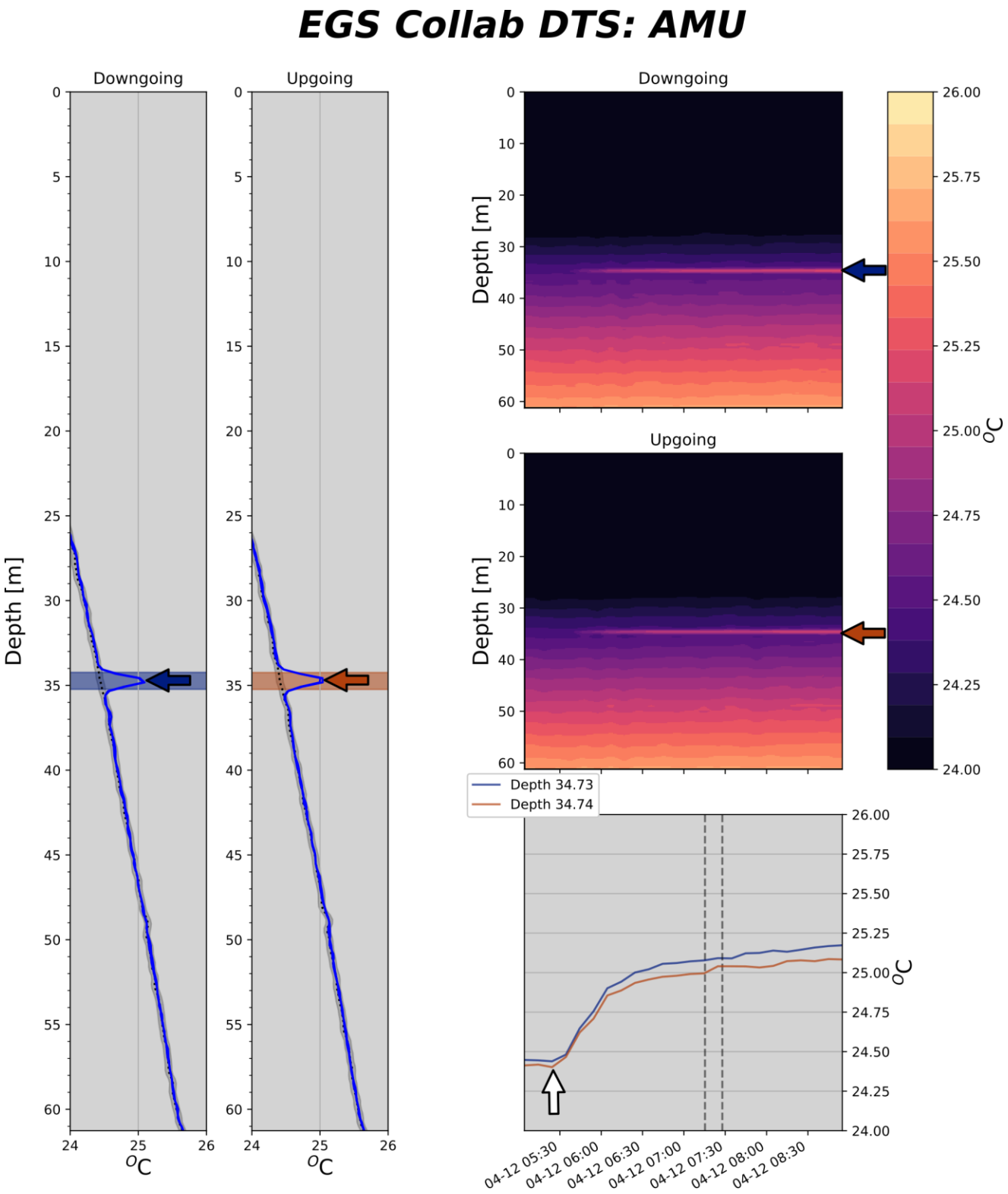

Figure 10. Temperature signal from the distributed temperature sensing (DTS) in monitoring well AMU showing a peak at a depth of about 35 m starting at about 5:30 UTC (white arrows). Blue and red arrows indicate the depth of the fracture on the downgoing and upgoing section of fiber, respectively. These colors correspond to the blue and red timeseries traces shown in the bottom right.

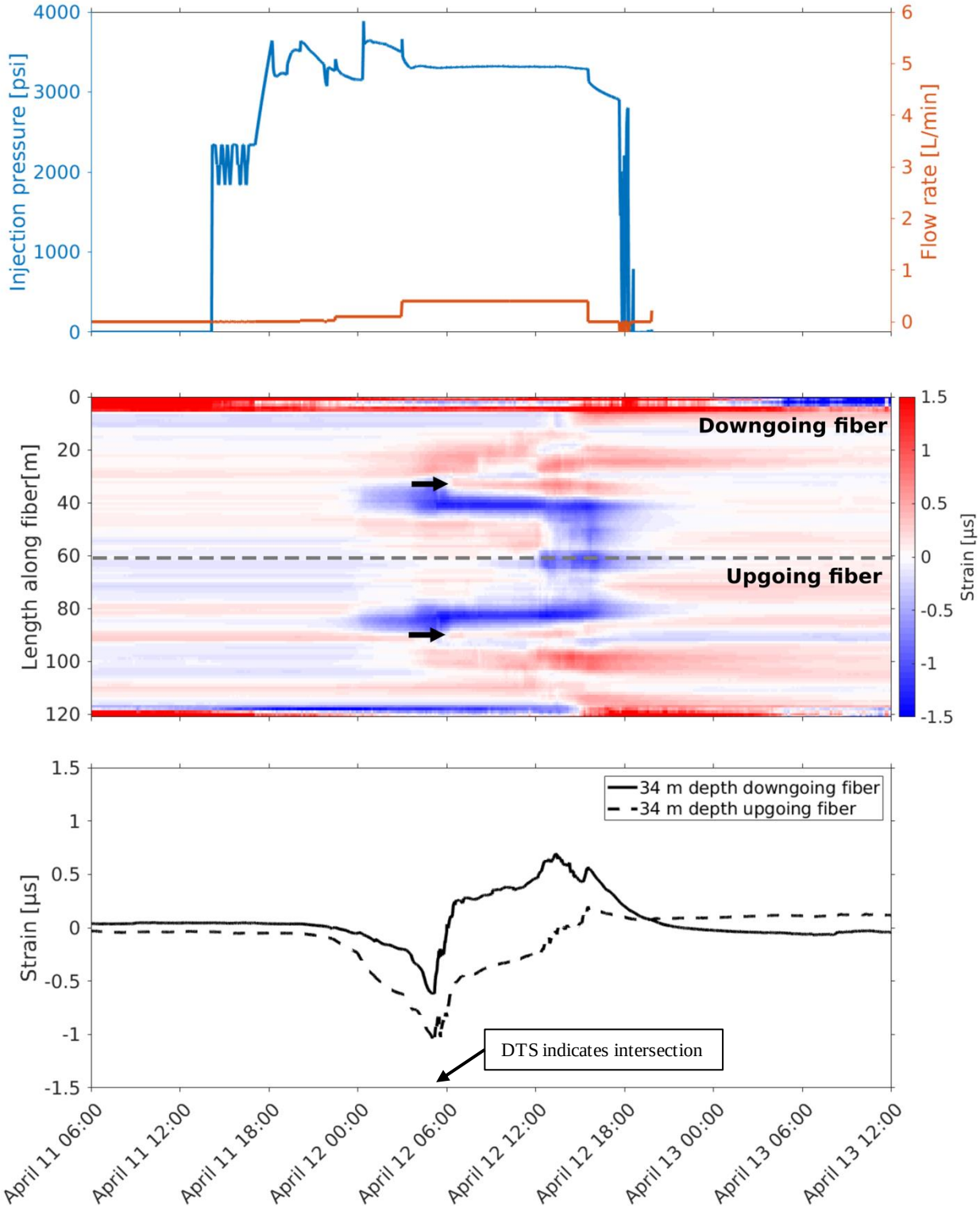

Figure 11. Low-frequency DAS strain recorded along borehole AMU during Stimulation 1 in Zone 7. (Top) Injection pressure and flow rate; (Center) Low-frequency DAS strain recorded along the length of the fiber deployed in borehole AMU. Note symmetry around the bottom of the well. Arrows indicate extensional signals indicating fracture hits at a depth of ~34 m, recorded on both sections of the fiber. (Bottom) Strain at ~34 m depth at the time of the observed DTS spike (5:23 am UTC) for both sections of the fiber.

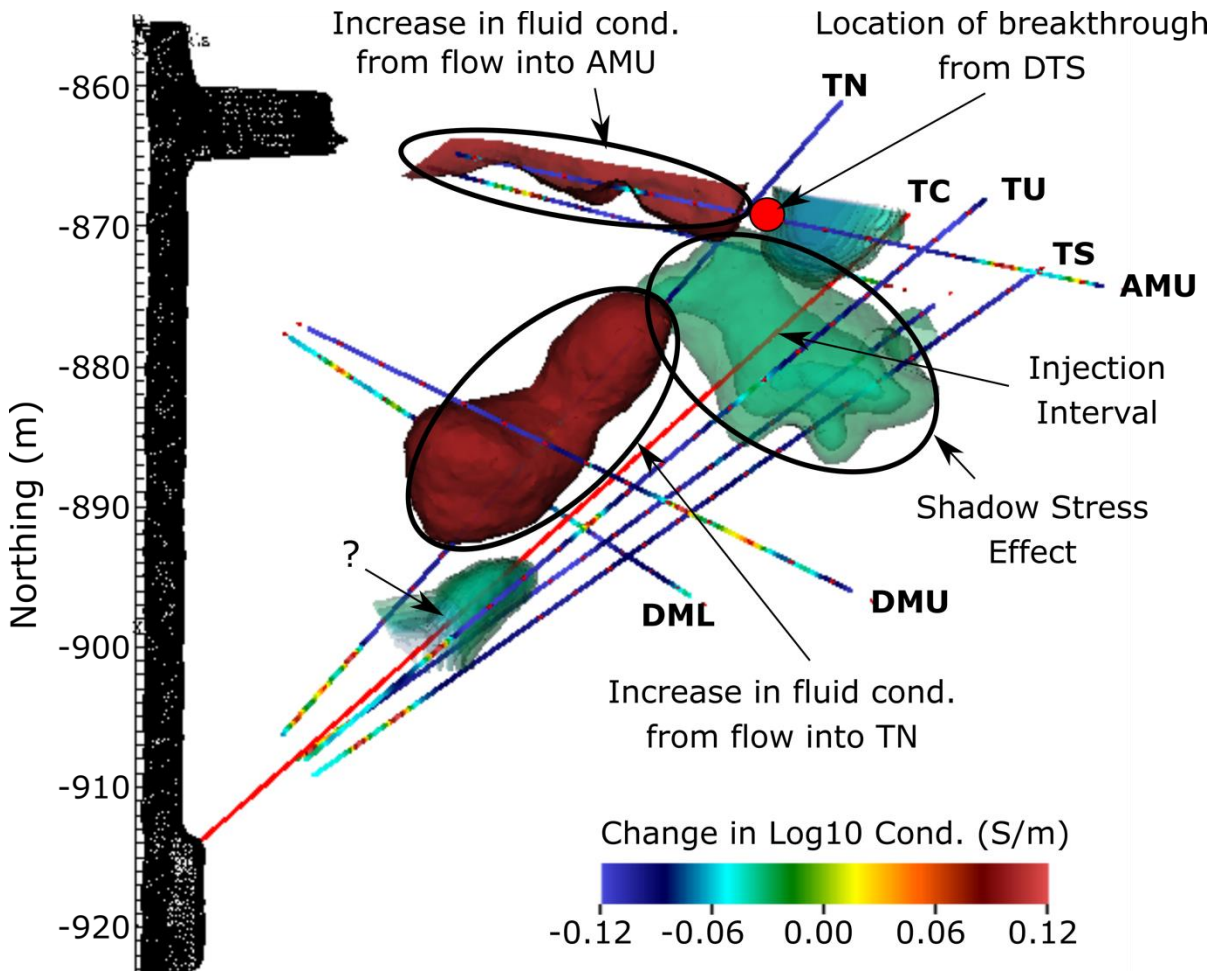

Figure 12. Preliminary electrical resistance tomography image of the testbed during Stimulation 1. Several things are notable: near the injection interval, a shadow stress feature is observed (green). Increases in conductivity are observed near well TN carrying produced water, and AMU, which the stimulated fracture penetrated.

Early on during this stimulation while the flowrate was very low (3 mL/min), the SIMFIP tool measured a consistent, mostly vertically downward displacement in short steps of few micrometers totaling about 20 microns starting at pressures between 2500 – 3000 psi, which is well below the breakdown pressure of ~3650 psi. At the breakdown at a pressure of ~3650 psi, an abrupt change in the directionality of the displacement of almost 90 degrees from mostly vertical down to north and slightly upwards occurred totaling about 5 micrometers, which was accompanied by a drop in pressure (with flow kept at a constant flowrate of 3 mL/min). This displacement was subsequently partially reversed, however an irreversible component in the direction of the initial step-wise displacements remained (Figure 13). The pattern of the displacements observed in combination with the initial pressure build up and subsequent drop could be an indication of the activation of a pre-existing fracture in a stick-slip-like shear mode preceding opening at breakdown and partial closing when pressure starts to drop again. The same step-wise displacement was not observed during later stages of the test.

The initial movement of the rock during stimulation was not indicated by the DORSA probe located in the TN borehole several tens of meters away. However, after flow was increased to 400 ml/min the DORSA started to exhibit a very linear but polyaxial contraction. This trend started to reverse after the injection was stopped (Figure 13). The contraction on the DORSA is in agreement with the negative strain measured by the DAS below the fracture intersection at 34m in AMU, indicating a compression of the rock mass. The DORSA was placed far away from where fractures intersected TN, therefore only measuring secondary fracturing effects. Interestingly, the DORSA was ideally placed for the later stimulation of Zone 1 and clearly showed fracture opening of approximately 200 micrometers when the fracture intersected and passed borehole TN.

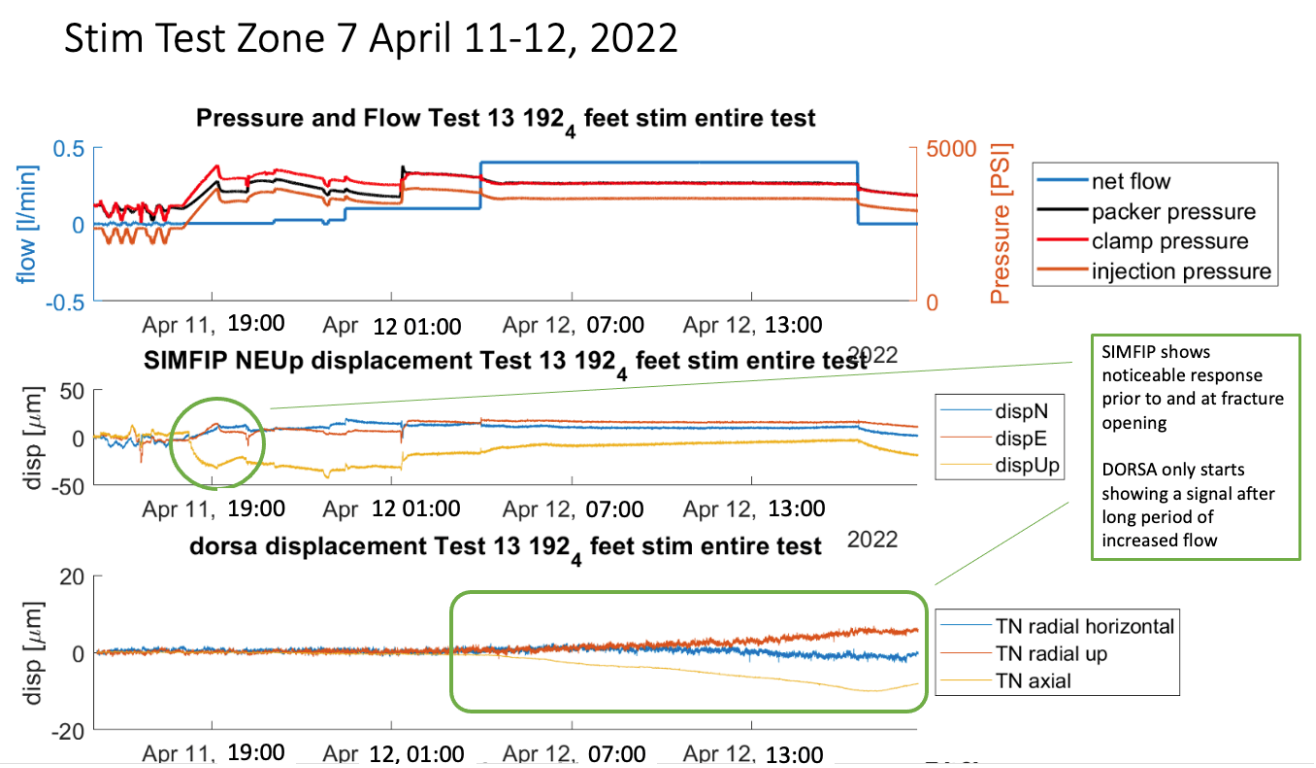

Figure 13. Displacements measured in TC and TN by the SIMFIP and DORSA probes during zone 7 stimulation.

5.2 TU Stimulation 177.4 - 179.6 ft. Interval

Simulations indicated that injection of fluid from TC would not be sufficient to observe a thermal breakthrough. Consequently, an attempt was made to stimulate a zone of borehole TU. TU was targeted for stimulation because it was the only well from which no significant production flow had been observed and it had a number of wells below it to possibly cage flow (Frash et al., 2018; Frash et al., 2021; Frash et al., 2020). On May 5, 2022, a stimulation was performed in TU (Figure 14) at a depth approximately aligned with Zone 4 of TC (see bottom panel of Figure 15 for injection parameters). Injection commenced at 1 L/min until breakdown was observed approximately 1 min later. A peak pressure of ~5500 psi was reached and flow was subsequently increased to 5 L/min and held for roughly 4 hrs. During this time, pressure approached a steady state value of 4500 psi. The resulting fracture intersected TC, TN, and TL and outflow from these boreholes totaled approximately 25% of the injected volume.

On May 6, 2022, injection into TU resumed at 5 L/min. While flowing into TU, the packer installed in TC was moved slightly because it appeared that a fracture from TC was impinging on the packer. Injection was then switched to TC at 2 L/min to identify whether flow from TC would be captured at TU. Outflow was measured from the packer intervals in TN and TU totaling ~35% of injection, representing a significant improvement in fluid recovery from previous TC injections.

During this phase of stimulation, no intersections were observed with the grouted monitoring boreholes via DTS. However, this phase of injection did produce the first detectable seismic events beginning with the restart of injection at 5 L/min on May 6 (Figure 15). Due to the low signal-to-noise ratio of the seismic events, automatic processing during the entire experiment did not produce reliable locations. We therefore manually revised all phase arrival picks, added S-wave arrivals (these were not included in the automatic workflow) and relocated the seismicity before interpreting the results. Figure 15 shows the timing and location of seismicity during this time period. Only nine events were detected and were located generally above and towards the drift from the injection point. This is consistent with the observations of flow at the grouted wells and drift during previous tests.

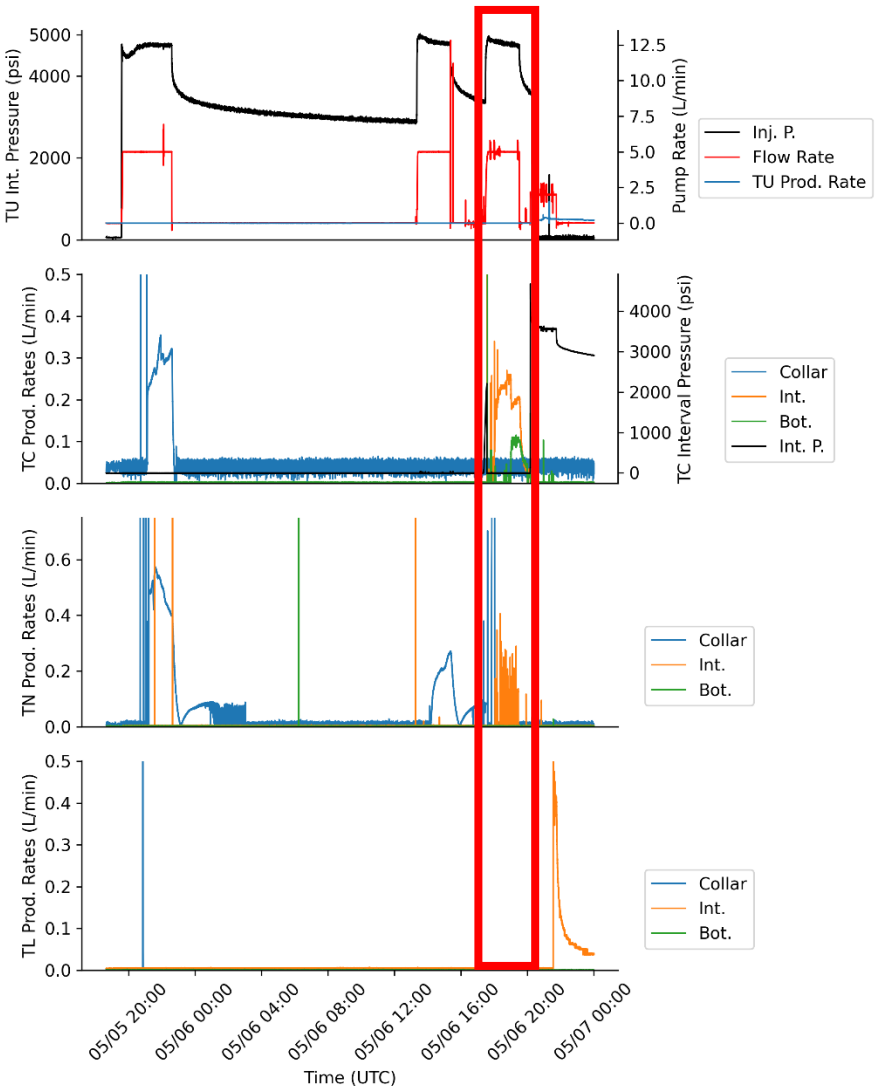

Figure 14. Plot of the stimulation data for the 177.4-179.6ft interval in well E2-TU on May 5 and May 6. Upper plot is the pump rate and interval pressure in well E2-TU. Note that for the last injection cycle the flow was directed into the interval of well E2-TC while water was produced from well E2-TU (red box). The bottom three plots show the recorded flow rates from the packed-off interval, zone below the interval (Bot.), and from the well collar for wells TC, TL, TN.

A plan view of the change in bulk conductivity caused by the TU-TC stimulations is shown in Figure 16. A positive conductivity anomaly, likely associated with an increase in porosity (i.e., fractures opening) appeared shortly after the TU injection on May 5th, with no further changes after the TC stimulation on May 6th. Alignment of the anomaly generally corresponds with the alignment of the microseismic events shown in Figure 15. Although the injection intervals in TC and TU were depressurized by May 7th, the positive conductivity anomaly persisted through to the next stimulation events in TU starting on May 17th.

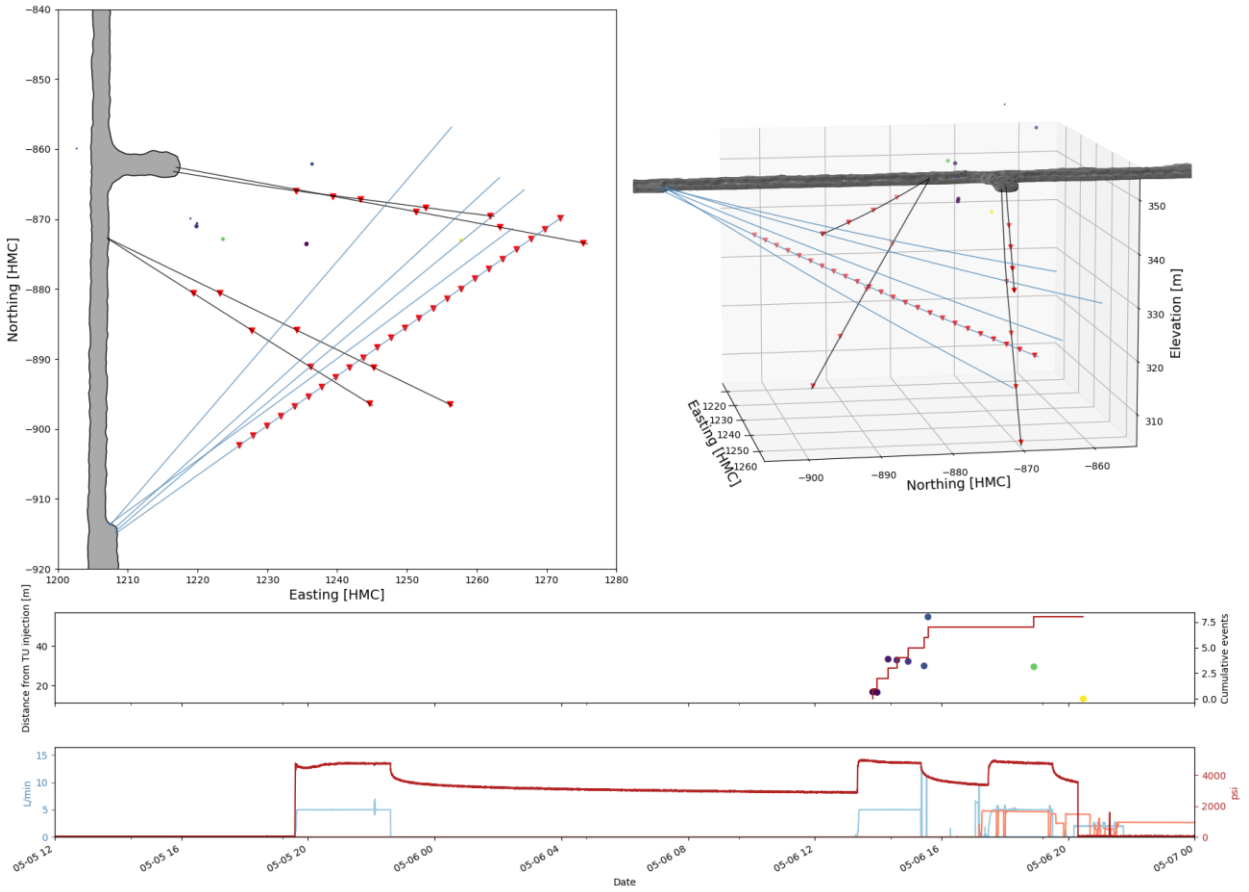

Figure 15. Earthquakes detected during stimulation of the 177.4 - 179.6 ft interval of TU. The top two panels show the location of each event. The uppermost timeseries plot shows the cumulative number of events and their distance from the injection point, with dot color changing with time. The bottom timeseries plot shows the injection pressure and flow rate in psi and L/min, respectively. The time axis is in UTC.

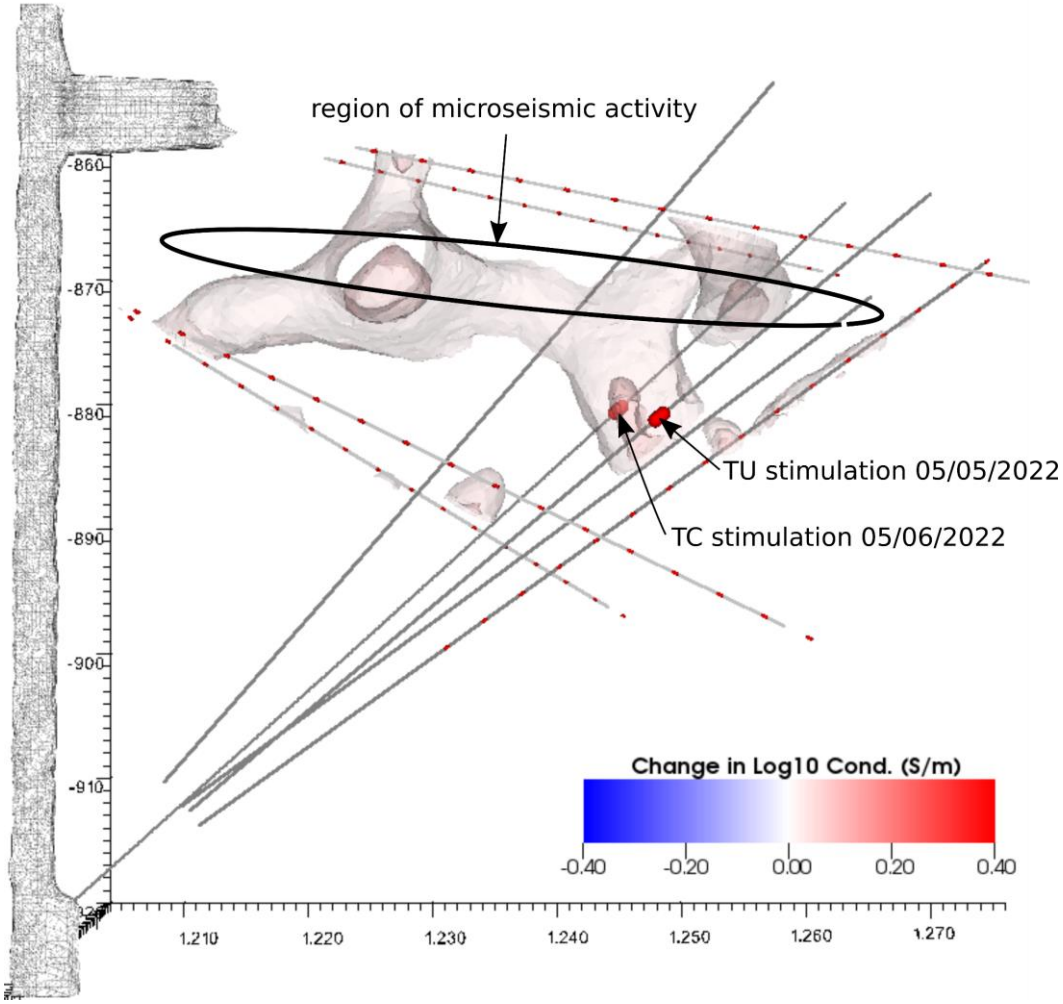

Figure 16. ERT-based change in bulk electrical conductivity from pre-stimulation on May 05 12:00, to post stimulation on May 7 00:00 (TU Zone 3). Increases in conductivity are likely caused by increases in porosity (e.g., fractures opening), and generally align with microseismic event locations shown in Figure 15. Negative changes in conductivity associated with compressive porosity reduction adjacent to the positive anomaly are not shown.

6. FLOW, TRACER, AND THERMAL CIRCULATION TESTING: 177.4 - 179.6 FT INTERVAL OF TU

Following the flow tests in the 177.4 - 179.6 ft interval of TU, flow tests were conducted in TC Zone 1 and TC Zone 3 on May 17 and May 18 respectively. The TC Zone 1 injection occurred at a nominal flowrate of 5 L/min for 5 hrs, followed by the TC Zone 3 injection at a nominal flowrate of 5 L/min for 12 hrs. During the latter injection in particular, significant changes in bulk conductivity developed within the test bed. Positive changes in conductivity, which are indicative of increases in porosity (i.e., fracture aperture dilation), originate near the Zone 3 injection point and extend north-northwest to connect to a nearly east-west trending anomaly that appears to extend to the drift outside of the ERT imaging zone. This general pattern of changes in conductivity is maintained for the remainder of the flow testing in TU as described below, including the saline tracer imaging and the final high-rate flow test. Negative changes in conductivity adjacent to the positive changes are presumably caused by compressive stresses that squeeze native pore water out of the rock and reduce pore space, thereby reducing bulk conductivity (Johnson et al., 2021).

Following the flow tests in TC Zones 1 and 3, the 177.4–179.6 ft interval in TU was selected as the injection zone for a long-term flow test, tracer testing, and then a thermal circulation test consisting of injection of chilled water. Injection began on May 19, 2022 at 2 L/min before being increased to 3 L/min on May 24 and then 3.4 L/min on 5-26. On May 19 and May 20 while flowing, packers installed in TC, TN, and TL were incrementally placed at various depths to better isolate and capture flow. A failure in the flow system occurred on 6/4, which resulted in a two-week hiatus in testing before the system was brought back online for an additional month of circulation testing (Figure 17).

Seismicity was again absent during the flow testing while injecting into TC, but resumed when injection was switched back to TU. Figure 18 shows the location and timing of the detected seismic events. From the start of the flow testing into TU until the flow system failure, more than 150 events were detected. Until May 26, these events loosely defined a structure striking ENE and dipping SSW, broadly consistent with a sigma-3-normal fracture or series of fractures that intersect the drift near the entry to the battery alcove.

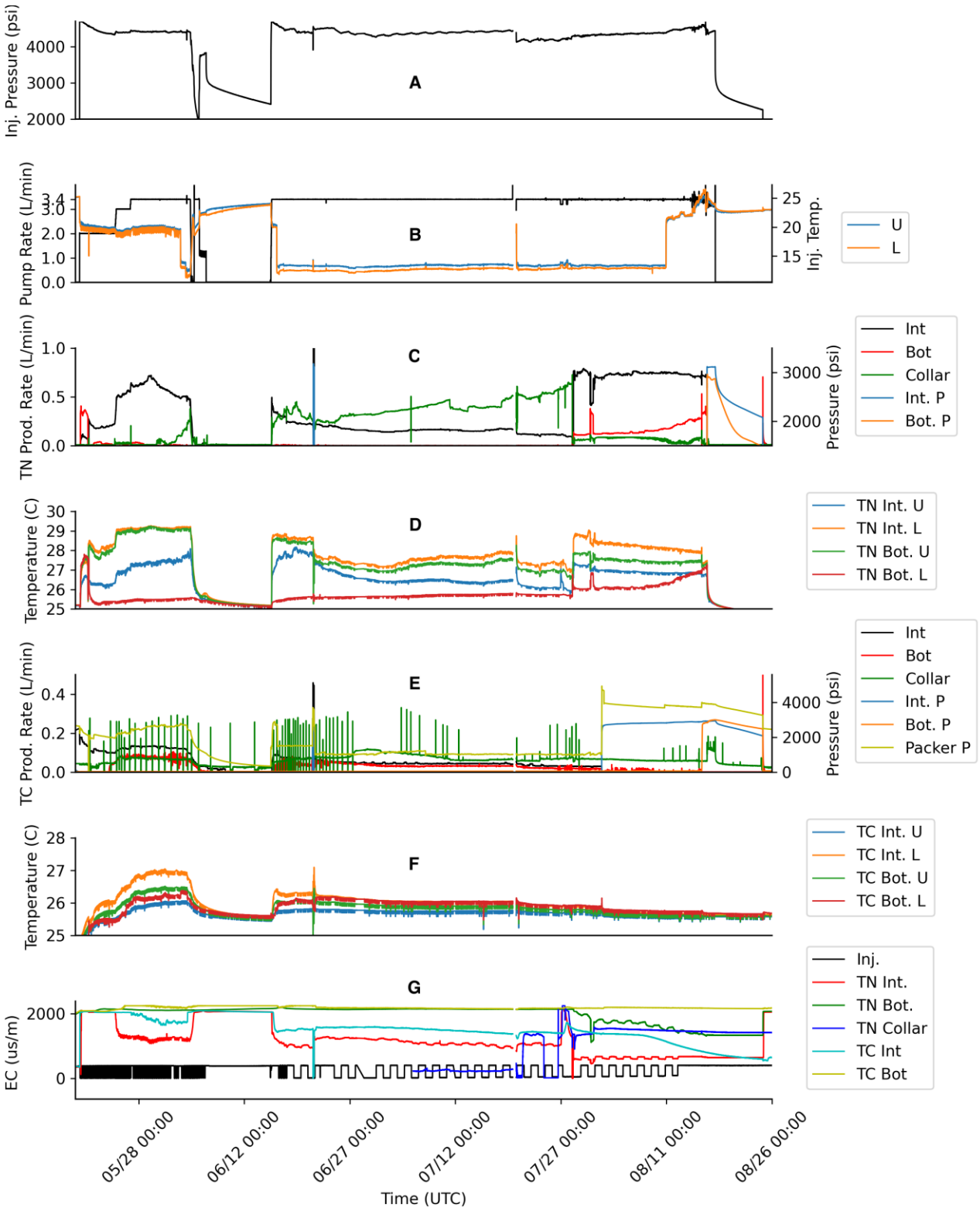

Figure 17. Top-tier parameters logged over the flow test. A - injection pressure, B – pump rate and two indications of the injection temperature, C – water production rates for the interval, bottom (below the interval), and collar regions of well TN, D – Temperatures in well TN in the packer interval and bottom, E – Water production rates from well TC from the interval, bottom, and collar, F – Temperatures in well TC in the interval and bottom, G – electrical conductivity of the injected water and produced water from the interval, bottom, and collar of well TN, and the interval and bottom of well TC. U and L mean upper and lower thermocouples that are at the top and bottom of the interval. P means pressure.

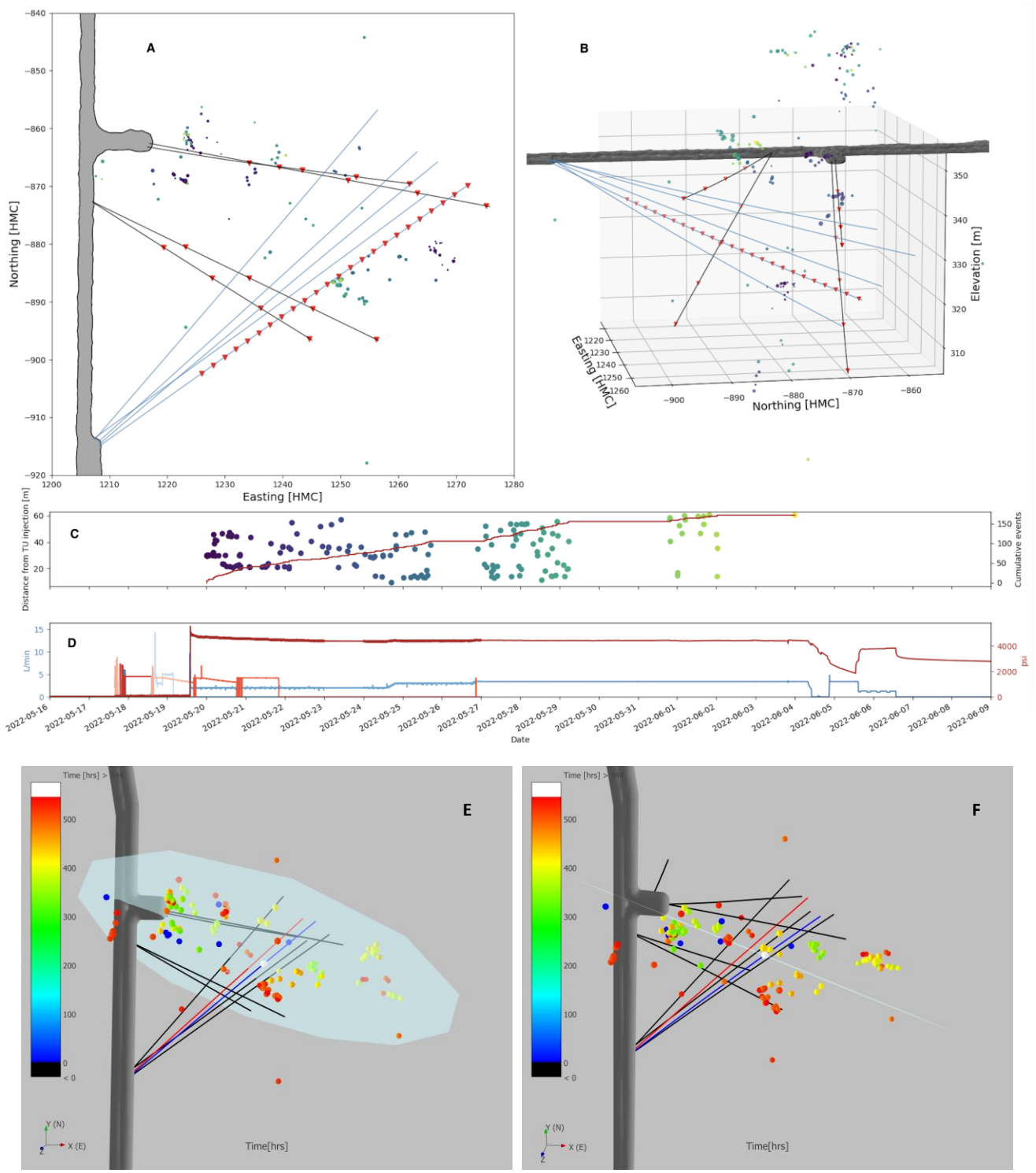

Figure 18. Earthquakes detected during flow testing into the 177.4 - 179.6 ft interval of TU. A and B show the location of each event. C shows the cumulative number of events and their distance from the injection point. D shows the injection pressure and flow rate in psi and L/min, respectively. The time axis is in UTC. E shows a plan view of a fracture fitted to the MEQs, and F provides a view parallel to the fitted fracture.

The start of flow testing in TU also produced a complex pattern of fracture intersections with the grouted monitoring boreholes, as shown by temperature measured on the DTS system and strain recorded on the DAS systems. Figure 19 shows the change in temperature at all four grouted boreholes relative to May 18, before the flow testing in TU began. Increases in temperature indicate flowing fracture intersections and are most abundant in DML, which is consistent with a generally SSW dipping fracture trends.

Difference ERT (Figure 20) shows a significant increase in conductivity, particularly in the region of microseismic activity identified in Figure 16 relative to just prior to injection on May 19. Figure 16 shows only the change in conductivity due to the previous injection. In Figure 20, early times, (panels A through C) show TS is filling with formation water. Over this time period conductivity increases in the same location during the stimulation shown in Figure 16. Even though the time increment is small, the conductivity increases significantly from panels C to D when the flowrate is increased from 2-3 L/min. There is relatively little change that occurs over the two-week period of no flow. This suggests either much of the system remained pressurized during the outage, or that the changes are slow to dissipate. Regions of decreasing conductivity adjacent to the regions of increased conductivity are thought to be caused by compressive stresses.

These data are also consistent with observations of seeps in the drift (Figure 21). At the beginning of the flow test, seeps into the drift were primarily in the area near the battery alcove. In general, ceiling drips appear in groups of multiple dripping points within ~10 square feet. These were subsequently collected by hanging tarps from the ceiling to a common collection point. Using tissue paper as a wick, wall weeps were collected to produce localized dripping points. As the test continued, seeps developed at locations south of the initial locations, and that trend continued over the duration of the flow test.

The flow test was completed and transitioned to shut-in testing. The shut-in test data are analyzed and interpreted separately (Schwering et al., 2023).

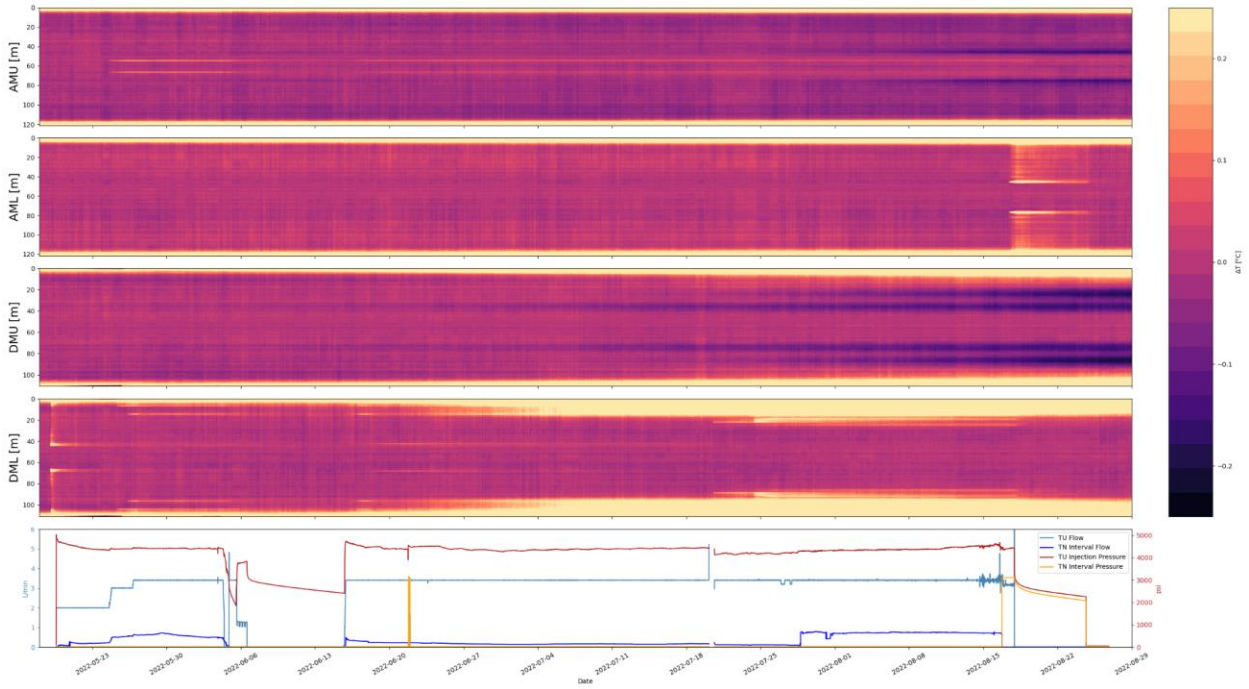

Figure 19. Change in temperature in each grouted borehole during the circulation test in TU. Each borehole is represented by a waterfall plot with hot colors representing temperature increases up to 0.25°C and dark colors decreases. The fiber package is installed as a loop going into and then back out of each borehole, so the y-axes represent distance along the fiber from the point where it enters until the point where it exits each borehole, thus the top half and bottom half of each panel are near mirror images of each other. The injection parameters are shown in the bottom panel for reference.

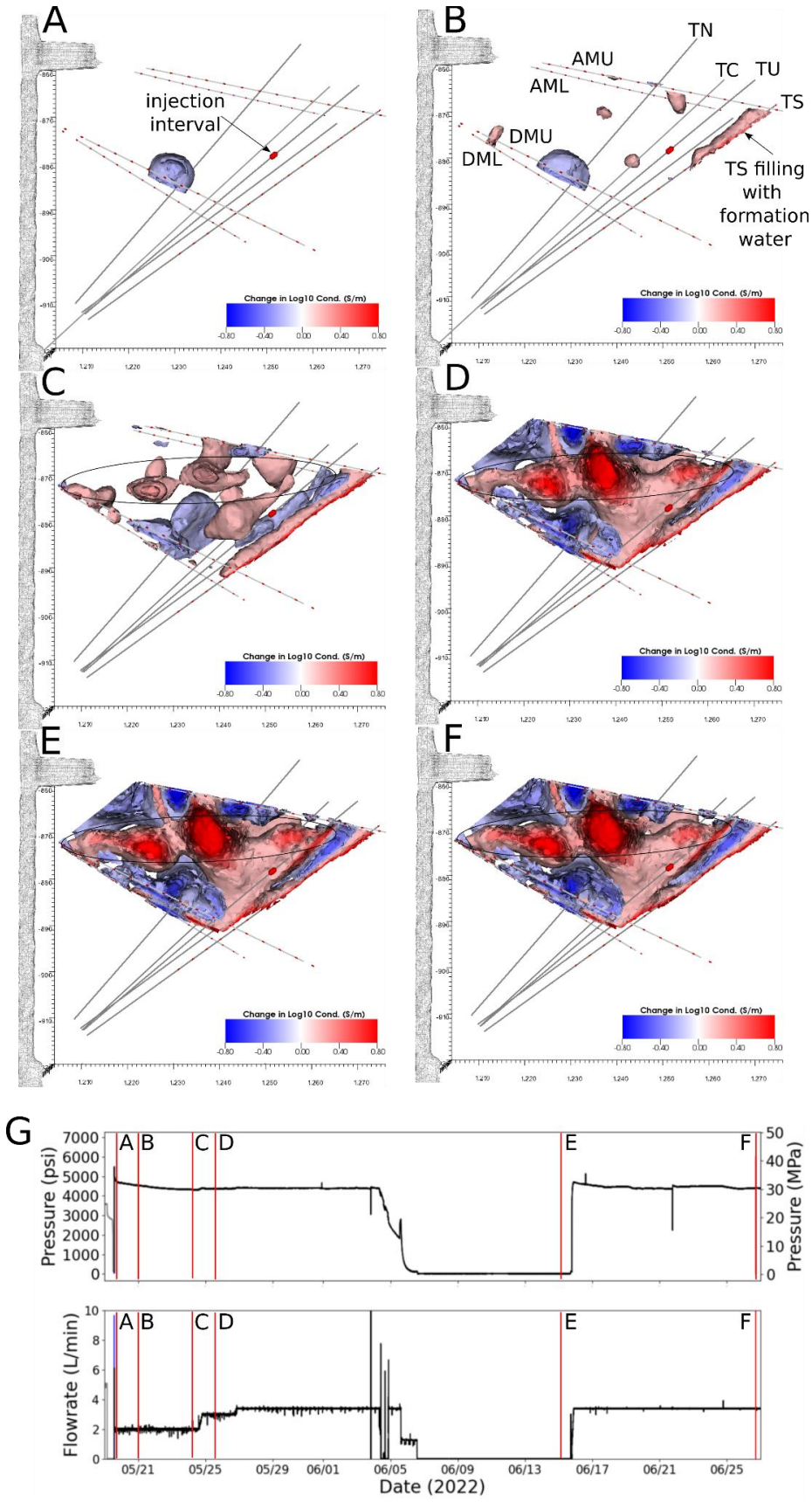

Figure 20. ERT imaging sequence showing changes in bulk conductivity during the TU 177.4 - 179.6 ft injection. Baseline ERT is just prior to injection on May 19, so these results do not show the total change in conductivity, only the changes caused by

this injection. A-F show the change in bulk conductivity at the times indicated in G. From time A-C, it is apparent that TS is filling with formation water, and the same anomaly from the TC injections is developing. A large increase in conductivity occurs from times C to D when the flowrate is increased from 2-3 L/min. Changes during the two-week flow outage are imperceptible (compare D and E), suggesting much of the system remained pressurized during the outage. Note that TS is the only borehole that did not contain a packer: the increases in conductivity around TS are likely caused by infilling of TS with formation water. Negative anomalies adjacent to the positive anomalies are presumably caused by compressive stresses. TC may also be infilling as suggested by the elongated positive anomaly along TC in C-F.

6.1 Tracer Tests and Water Balance

Mattson et al. (2023) discuss the water balance and the behavior of tracers in the E2/3 testbed during the flow test. Fluorescein, rhodamine B (a sorbing tracer), and sodium chloride were used as tracers. Tracers were detected at a number of locations within the production wells, two grouted monitoring wells, ceiling drips, wall weeps, and the floor. Based on the tracers and bulk water measurements, Mattson et al. (2023) conclude that most of the injected water was collected, however a large fraction of the water entered the drift through the floor, where the ability to collect, quantify, and analyze water was limited to somewhat crude bulk measurements. Water measurements from ceiling drips and wall weeps suggest a dynamic flow system where drift outflows shifted location with time. Fluorescein tracer breakthrough curves were used to determine travel time to the production wells and various parts of the drift. These results suggest a main fast flow pathway from the injection point in TU to the alcove/drift intersection with a series of secondary fractures with slower transport.

One tracer test will be briefly discussed here – the sodium chloride test. Throughout the flow test, the electrical conductivity of the injected water was changed in a step function as the reverse osmosis system was systematically turned on and off (Figure 17 G). The changes in electrical conductivity are observed in several of the production wells. It was hypothesized that the ERT system might also detect these changes, but the impact was smaller than desired. Injecting sodium chloride, however, could strongly affect the conductivity of the injected water. On July 26th, a saline tracer was injected into the TU 177.4 - 179.6 ft interval for approximately 8 hrs. Fluid conductivity of the tracer was approximately 75 times greater than the water the being produced to provide a high conductivity target for time-lapse ERT imaging. Figure 22 shows the change in bulk electrical conductivity caused by the tracer after the bulk conductivity had reached a steady state on July 27th. In the ERT difference image, the tracer appears to originate from TC at the location where a connection between TU and TC (TC Zone 3) was created on April 5th and 6th (Figure 8), suggesting a strong flow connection from TU to TC Zone 3. Tracer injected at TU 177.4 - 179.6 may not be visible in the ERT image due to poor data sensitivity in that location. However, from the injection point the tracer appears to travel in a well-defined path northwest toward well AMU, where the tracer then migrates southwest to the shallow regions of DML and DMU. The largest increase in bulk conductivity occurs near DML and DMU. The flow patterns indicated by the ERT imaging are consistent with observed outflows along the drift as shown in Figure 20 and Figure 21. A smaller anomaly occurs in the north-eastern part of the image. This appears to emanate from tracer flowing into TS, and moves eastward and downward in the formation.

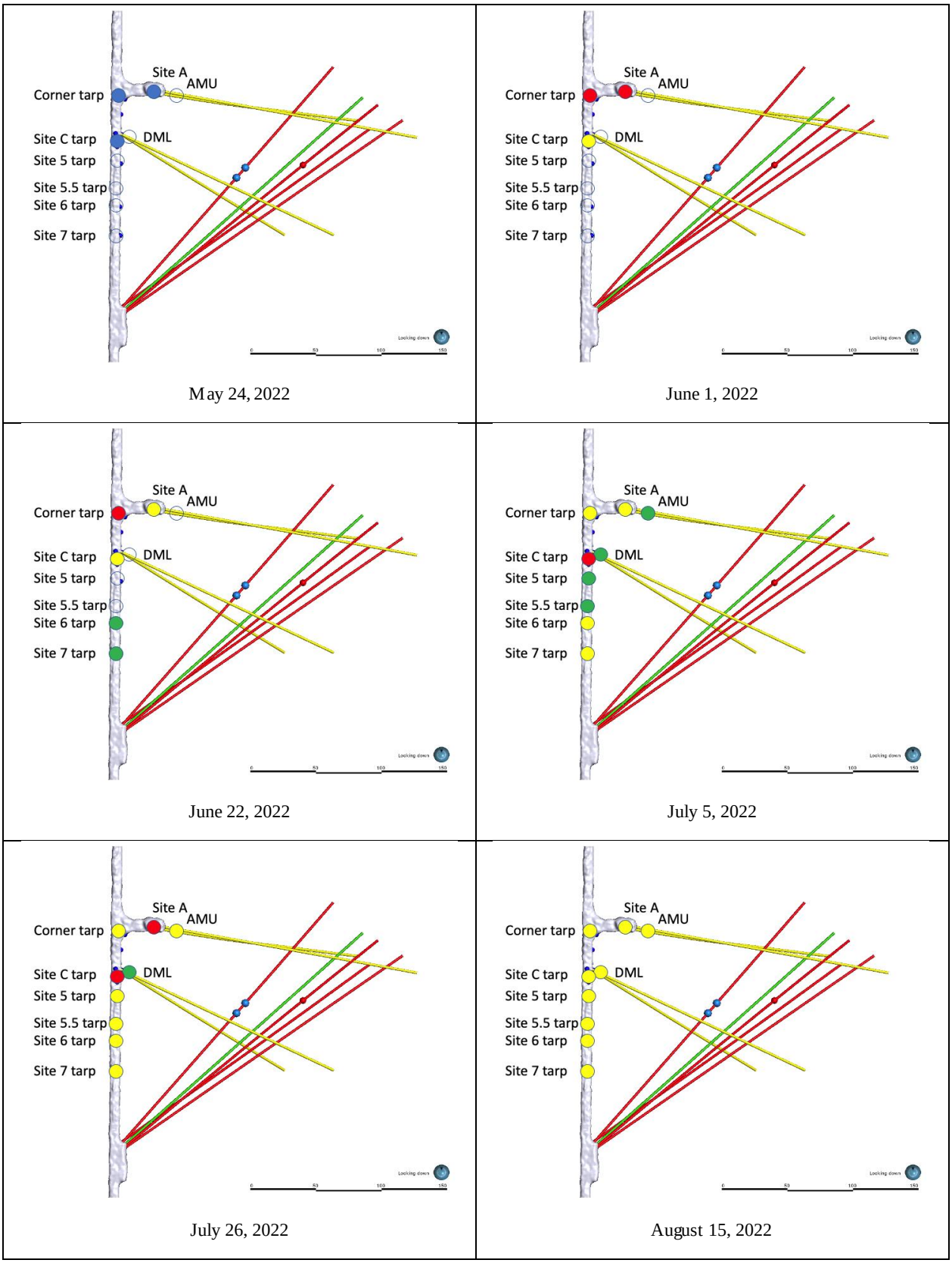

Figure 21. Subjective observations of drilling from the drift ceiling over time. Empty circles represent nonflowing collection locations, blue dots are initial collection locations, green dots represent increasing discharge over the previous observation, yellow - staying steady, and red - reduced discharge.

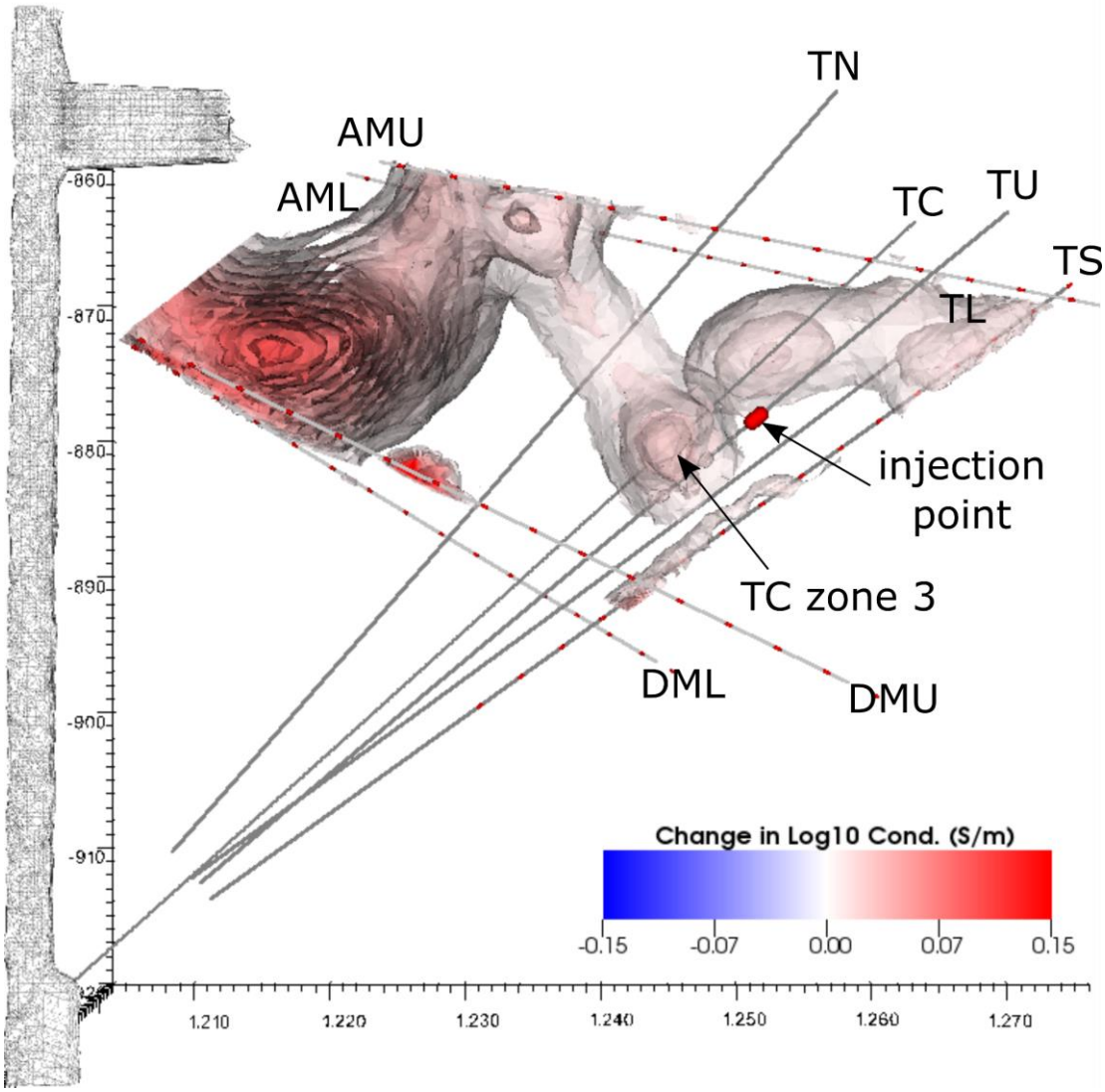

Figure 22. ERT Image of saline tracer distribution after injection at TU 177.4 - 179.6 ft for approximately 16 hours.

7. LESSONS LEARNED AT THE SCALE OF OUR EXPERIMENTS, LESSONS APPLICABLE TO EGS AT THE FULL SCALE

The motivation of the project was to build a collaborative experiment and model comparison project, allow data comparison to reservoir model predictions, and provide data for validation of predictions using ~10 m-scale field experiment data. The data were to include in-depth fracture characterization and well-performed well-monitored experiments collecting high-quality data using comprehensive instrumentation. A goal was to elucidate the basic relationship between permeability enhancement and stress, seismicity, and other parameters. Secondarily, the EGS Collab Project was tasked with facing and addressing problems that will occur, and to improve tools for EGS for the prediction of EGS development and performance. We sought to achieve the objectives of the EGS Collab Project by studying rock mass response to stimulation using accessible deep rock. We performed 10-m spatial scale experiments under stresses relevant to EGS (at 1.25 and 1.5 km depth) in crystalline rock. Our tests and analyses were performed to support the validation of thermal-hydrological-mechanical-chemical (THMC) modeling approaches. In addition, the EGS Collab project tested and improved novel and conventional field monitoring tools. By observation of system behavior during our experiments, we gained insight into permeability enhancement and evolution in crystalline rock. These observations and interpretations provide understanding of creating sustained and distributed permeability for heat extraction by generating new fractures that complement existing fractures.

The correlation between seismicity and permeability remains elusive. In E3, much of the seismicity that could be detected occurred in the upper regions of the testbed, even above the drift. Flow on the other hand apparently concentrated in the lower regions of the test bed and is predominantly thought to enter the drift from the floor. In E1, seismicity identified opening along many planes that were confirmed to be hydraulically conductive. ERT data however showed that a large fraction of the flow occurred where little seismicity occurred. Seismicity occurs when energy is released in the rock, for example from fracture tips or unmatching asperity contacts from different sides of a fracture hitting each other during shear. The seismicity does not necessarily identify that the pathways are large or viable for conveying fluid. Previously open pathways can take significant flow without inducing any new seismicity. Despite these challenges, microseismic

monitoring proved to be a valuable tool for understanding the in-situ fracture behavior in a way that is directly relevant to full scale EGS. In other words, microseismic data was shown to be highly valuable for confirming the stimulation of fractures, but that the absence of seismicity does not confirm the absence of flow. In the instance of the particular test bed employed in this project, the data may point to a scenario wherein new fractures tend to be more prone to the generation of MEQ's whereas the ERT responded to larger flows in the existing fractures. In practice, this suggests that larger-scale thermal developments relying heavily on the existence of MEQ's may be missing important components of the flow system. One of the key challenges faced in developing EGS reservoirs is to create distributed permeability throughout the reservoir to facilitate efficient thermal transfer of heat to the circulating fluid (e.g., (Doe et al., 2022; Grant, 2016)), so it is critical to understand where flow is actually occurring.

Our flow systems were distributed and dynamic. In both E1 and E3 we hydraulically fractured the rock and connected our injection and production wells. In addition, the stimulated flow system connected to many other locations beyond the intended testbed, resulting in reduced recovery rates for the injected fluid at the production wells, especially when the connection between the injection well(s) and production well was minor. It is not known how this would impact fracture caging in a full-scale EGS system having many differences from the EGS Collab test beds. Whether connecting to an existing fracture network or creating new fractures, flow was observed and quantified at numerous locations away from where flow was expected. If this is the general case, this could possibly be good for EGS because it increases heat transfer area between the fluid and rock. More diffuse flow may also pose a greater risk for injection-induced seismicity when closed-loop flow is not attained. These questions require further study. All of our tests were performed under nonlithostatic stress gradients. These gradients may have impacted flow direction, however 25% - 90% of our injected water was recovered in E1 and E3. Throughout all of our experiments, flow rates from the many collection locations were always changing even when injection rates were constant. In E1, resuming pumping after any stop typically resulted in a decrease to the injection pressure required for a constant rate of injection. In E2, this same action appeared to relate to an increase in the injection pressure. Tracer studies indicated changes in flow paths over time and in response to stopping or changing the flow rate. Full-scale EGS will also have complications due to stress gradients applied from injection, production, and temperature changes, the injection and later degradation of proppants, and dynamic flow networks that will change over time and in response to varying injection and production rates and fouling processes. The role of the uncertain and heterogeneous stress gradients should be carefully considered, especially with respect to the imperfect prediction of propagation direction of hydraulically stimulated fractures. The EGS Collab project highlighted the current inability to accurately predict the behavior of a planned EGS stimulation due to irreducible uncertainties and heterogeneity in the rock. Although changes in the mechanical properties of the rock mass may be due to stresses induced by pumping, modeling shows that thermal gradients created by the presence of the access drifts can greatly affect the trajectories of induced fractures. In the EGS Collab tests, the temperature changes associated with the water being introduced into the reservoir are probably too subtle to have major effects, but larger scale operations may be affected by these types of temperature gradients, particularly in conjunction with infill drilling and refracturing.

There are many possible explanations for a dynamic system, and these may operate together. These include geomechanical, geochemical, and biological processes. The geomechanical argument is that our systems were operated at pressures exceeding the minimum principal stress. Flow entering a fracture would exert a force on the rock blocks on either side of the fracture impacting the overall stress distribution. This force could open fractures to an extent. When flow reached another intersecting fracture, the force balance and directions would change, altering system apertures and flow, and changing flow paths. It is not clear whether pressure exceeding the minimum principal stress is required for this since under proper conditions shear stimulation occurs below the minimum principal stress. Biological processes are unlikely but possible in geothermal systems, and this also needs consideration. Microbes could grow in our system (Zhang et al., 2020) where conditions are right, and change flow paths through biofouling. During early test bed characterization, random wells would biofoul as seen in the optical logs, requiring the boreholes to be scrubbed; this process may have been accentuated by introducing oxygenated waters into a reducing environment. One would expect that as the microbes grow that the conditions would change as nutrients were consumed, that communities would flourish elsewhere impacting flow there. These flow path alterations would impact the pressures on rock blocks perhaps accentuating geomechanical processes. Geochemical processes cause dissolution and precipitation of solid phases that will impact permeability. Dissolution could concentrate flow as apertures increase, and this process could be self-enhancing. It is important to realize that for both biological and geochemical processes, that there are immense numbers of kinds of microbes and mineral phases. Considering single phase or single organism systems can be informative but is excessively limiting and possibly misleading. Biological processes are less likely to occur under elevated (>150°C) temperature conditions, but such conditions will increase geochemical reaction rates.

The management of our simple systems was complex. It required exercising a number of models from conceptual to numerical that had to be changed constantly to adapt to new responses from known or unknown stimuli. The experience indicates that successful reservoir management at any scale must be an active process requiring attention to and integration of important data streams. When interpreting multiple data sources of various types, we found that it was valuable to employ a wide-range of data sources, data analytics (e.g., inversion models, mapping, data integration, and machine learning methods), visualization methods, and a broad-spectrum of subject-matter expertise to best interpret this information. Using this process in an open forum enabled our team to obtain the most comprehensive understanding of what we were observing, the most likely causes of the observations, and potential solutions to remedy the problems that were encountered.

The limited permeability shown by many crystalline rock masses is well-represented by the rocks of the current test beds. Division of the rock mass into separate reservoirs, often by high-angle fracture systems can result in different fluid pressures between those reservoirs depending upon the frequency of fracturing. Therefore, extrapolation of results from one of the separate reservoirs to an entire geothermal field should be done with care unless good reasons can be made to assume a sufficient number of fractures or fracture systems exist to allow communication.

We did not establish flow systems at pressures below the minimum principal stress in either test bed. This does not mean shear stimulation below the minimum is not possible, however. In test bed 2 healed or filled fractures would not open below the minimum stress. The test bed lacked naturally conductive fractures that might have shear stimulated. Naturally conductive fractures elsewhere at the 4100 level were avoided over concerns that they might produce excessive flow to the underground openings. We did not conclusively establish thermal breakthrough in either of our flow tests. Thermal breakthrough could have occurred at higher-flow weep locations where temperature was not monitored. Additionally, we encountered Joule-Thomson effects which caused temperature increases as the water depressurized from the fractures to the wells. Had warm water been used in the flow tests, perhaps even greater initial misinterpretation might have occurred.

Ultimately, this experiment series represents a direct confrontation with the THMC challenges associated with EGS that provides critical insights at the fundamental science level. Predictions, and often assumptions of behavior going into these experiments were often defied during execution and had to be addressed through a continuous cycle of hypothesis, modeling, field trial, data analysis, interpretation of processes, and re-evaluation of understanding. This practice was constantly performed in a remote and challenging environment and is relevant for commercially viable EGS power production. Full-scale EGS applications will similarly have to confront the realities of stress/geologic heterogeneity, stimulated fracture propagation mechanics, the influence of natural fractures and geologic structure, evolving permeability pathways due to physical and chemical effects over time, and optimization of thermal circulation/conductivity. These challenges were commonplace for the five-year duration of EGS Collab activities at SURF and it is reasonable to expect similar of EGS work at the full scale. This project provided new insights, crucial observations, valuable updates to models, and a suite of both novel and commonplace stimulation, circulation, characterization, and monitoring tools/techniques to reduce uncertainties and increase the probability of success for EGS applications. Researchers and practitioners should be encouraged to build upon both the successes and the unsolved complexities that the EGS Collab Team illuminated within the underground mine workings at SURF.

ACKNOWLEDGMENTS

This material was based upon work supported by the U.S. Department of Energy, Office of Energy Efficiency and Renewable Energy (EERE), Office of Technology Development, Geothermal Technologies Office, under Award Number DE-AC02-05CH11231 with LBNL and other awards to other national laboratories. The United States Government retains, and the publisher, by accepting the article for publication, acknowledges that the United States Government retains a non-exclusive, paid-up, irrevocable, world-wide license to publish or reproduce the published form of this manuscript, or allow others to do so, for United States Government purposes. Sandia National Laboratories is a multimission laboratory managed and operated by National Technology & Engineering Solutions of Sandia, LLC, a wholly owned subsidiary of Honeywell International Inc., for the U.S. Department of Energy's National Nuclear Security Administration under contract DE-NA0003525. Portions of this work were performed under the auspices of the U.S. Department of Energy by Lawrence Livermore National Laboratory under Contract DE-AC52-07NA27344. This paper describes objective technical results and analysis. Any subjective views or opinions that might be expressed in the paper do not necessarily represent the views of the U.S. Department of Energy or the United States Government. The research supporting this work took place in whole or in part at the Sanford Underground Research Facility in Lead, South Dakota. The assistance of the Sanford Underground Research Facility and its personnel in providing physical access and general logistical and technical support is gratefully acknowledged. We also thank the crew from RESPEC, who logged the core upon recovery from drilling, and also supported the wireline logging operations. The earth model output for this paper was generated using Leapfrog Software, copyright Seequent Limited. Leapfrog and all other Seequent Limited product or service names are registered trademarks or trademarks of Seequent Limited.

REFERENCES

1. Augustine, C. (2016). Update to Enhanced Geothermal System Resource Potential Estimate. *GRC Transactions, 40*, 6.
2. Blackwell, D. D. (1967). *Terrestrial heat-flow determinations in the northwestern United States*. (Ph.D.). Harvard University,
3. Burghardt, J., Doe, T., Ingraham, M., Schwering, P., Ulrich, C., Roggenthen, W. M., Reimers, C., & EGS Collab Team. (2020). *Integration of Shut-In Pressure Decline, Flow back, Hydraulic and Sleeve Re-Opening Tests to Infer In-Situ Stress*. Paper presented at the 54th U.S. Rock Mechanics/Geomechanics Symposium.
4. Burghardt, J., Knox, H. A., Doe, T., Blankenship, D., Schwering, P. C., M., I., Kneafsey, T. J., Dobson, P. F., Ulrich, C., Guglielmi, Y., & Roggenthen, W. (2022). *EGS Stimulation Design with Uncertainty Quantification at the EGS Collab Site*. Paper presented at the 56th US Rock Mechanics/Geomechanics Symposium, Santa Fe, New Mexico, USA.
5. Clark, S. P., Jr. (1966). Section 21. Thermal Conductivity. In *Handbook of Physical Constants* (pp. 459-482): Geological Society of America.
6. Dobson, P., Kneafsey, T., Morris, J., Singh, A., Zoback, M., Roggenthen, W., Doe, T., Neupane, G., Podgorney, R., Wang, H., Knox, H., Schwering, P., Blankenship, D., Ulrich, C., Johnson, T., White, M., & EGS Collab Team. (2018). *The EGS Collab Hydroshear Experiment at the Sanford Underground Research Facility – Siting Criteria and Evaluation of Candidate Sites*. Paper presented at the Geothermal Resources Council 2018 Annual Meeting, Reno, NV.
7. Doe, T., Riahi, A., Fu, P., Damjanac, B., Sonnenthal, E., Finnila, A., Kennedy, M. B., & Blankenship, D. (2022). *Performance evaluation of engineered geothermal systems using discrete fracture network simulations*. Paper presented at the 47th Workshop on Geothermal Reservoir Engineering, Stanford University, Stanford, California.
8. Frash, L. P. (2021). *Geothermal Design Tool (GeoDT)*. Paper presented at the 46th Workshop on Geothermal Reservoir Engineering, Stanford University, Stanford, California.
9. Frash, L. P. (2022). Geothermal Design Tool. https://github.com/GeoDesignTool/GeoDT.
10. Frash, L. P., Fu, P., Morris, J., & EGS Collab Team. (2018). *Fracture Caging: Can We Control the Extent of a Hydraulic Fracture Stimulated Zone?* Paper presented at the 43rd Workshop on Geothermal Reservoir Engineering, Stanford University, SGP-TR-213.

11. Frash, L. P., Fu, P., Morris, J., Gutierrez, M., Neupane, G., Hampton, J., Welch, N. J., Carey, J. W., & Kneafsey, T. (2021). Fracture Caging to Limit Induced Seismicity. *Geophysical Research Letters, 48*(1), e2020GL090648. doi:https://doi.org/10.1029/2020GL090648
12. Frash, L. P., Hampton, J. C., Gutierrez, M. S., & EGS Collab Team. (2020). *Fracture Caging to Control Induced Seismicity with Inspiration from the EGS Collab Project*. Paper presented at the 45th Workshop on Geothermal Reservoir Engineering, Stanford University, Stanford, California.
13. Frash, L. P., Li, W., Meng, M., Carey, J. W., & Sweeney, M. (2022). *Enhanced Geothermal System Design Using GeoDT and Fracture Caging — EGS Collab Stimulation Prediction Study*. Paper presented at the 56th U.S. Rock Mechanics/Geomechanics Symposium. https://doi.org/10.56952/ARMA-2022-0278
14. Grant, M. A. (2016). Physical performance indicators for HDR/EGS projects. *Geothermics, 63*(2-4).
15. Guglielmi, Y., Cappa, F., Avouac, J.-P., Henry, P., & Elsworth, D. (2015). Seismicity triggered by fluid injection–induced aseismic slip. *Science, 348*(6240), 1224.
16. Guglielmi, Y., Cook, P., Soom, F., Dobson, P., Kneafsey, T., Valley, B., Kakurina, M., Niemi, A., Tsang, C. F., Tatomir, A., Juhlin, C., & Basirat, F. (2021a). *Estimating Stress from Three-Dimensional Borehole Displacements Induced by Fluid Injection in Different Types of Fractured or Faulted Rocks*. Paper presented at the 55th US Rock Mechanics/Geomechanics Symposium, Houston, Texas, USA.
17. Guglielmi, Y., Cook, P., Soom, F., Schoenball, M., Dobson, P., & Kneafsey, T. (2021b). In Situ Continuous Monitoring of Borehole Displacements Induced by Stimulated Hydrofracture Growth. *Geophysical Research Letters, 48*, e2020GL090782. doi:https://doi.org/10.1029/2020GL090782
18. Guglielmi, Y. G., Cappa, F., Rutqvist, J., Tsang, C. F., Wang, J., Lançon, H., Durand, J., & Janowczyk, J. B. (2014). *Step-Rate Injection Method for Fracture In-Situ Properties (SIMFIP): Monitoring Fractures Stimulation Efficiency*. Paper presented at the 48th U.S. Rock Mechanics/Geomechanics Symposium, Minneapolis, Minnesota.
19. Heise, J. (2015). The Sanford Underground Research Facility at Homestake. *Journal of Physics: Conference Series, 606*(1), 26.
20. Ingraham, M. D., Schwering, P. C., Burghardt, J., Ulrich, C., Doe, T., Roggenthen, W. M., & Reimers, C. (2020). *Analysis of Hydraulic Fracturing on the 4100 Level at the Sanford Underground Research Facility*. Paper presented at the 54th U.S. Rock Mechanics/Geomechanics Symposium. https://doi.org/
21. Johnson, T. C., Burghardt, J., Strickland, C., Knox, H., Vermeul, V., White, M., Schwering, P., Blankenship, D., & EGS Collab Team. (2021). 4D Proxy Imaging of Fracture Dilation and Stress Shadowing Using Electrical Resistivity Tomography During High Pressure Injections Into a Dense Rock Formation. *Journal of Geophysical Research: Solid Earth, 126*(11), e2021JB022298. doi:https://doi.org/10.1029/2021JB022298
22. Kneafsey, T., Blankenship, D., Burghardt, J., Johnson, T., Dobson, P., Schwering, P. C., Strickland, C., Vermuel, V., White, M., Morris, J. P., Fu, P., Ingraham, M., Roggenthen, W., Hopp, C., Tribaldos, V. R., Guglielmi, Y., Knox, H., Cook, P., Soom, F., Doe, T., Ulrich, C., Ajo-Franklin, J. B., Huang, L., Neupane, G., Pyatina, T., Weers, J., & Team, T. E. C. (2022a). *The EGS Collab – Experiment 2 Stimulations at 1.25 km Depth*. Paper presented at the Geothermal Rising Conference, Reno, NV.
23. Kneafsey, T., Blankenship, D., Dobson, P., Burghardt, J., White, M., Morris, J. P., Johnson, T., Ingraham, M., Ulrich, C., Roggenthen, W., Doe, T., Smith, M., Ajo-Franklin, J. B., Huang, L., Neupane, G., Pyatina, T., Schwering, P. C., Hopp, C., Tribaldos, V. R., Guglielmi, Y., Strickland, C., Vermuel, V., Fu, P., Knox, H. A., & EGS Collab Team. (2022b). *The EGS Collab – Initial Results from Experiment 2: Shear Stimulation at 1.25 km depth*. Paper presented at the 47th Workshop on Geothermal Reservoir Engineering, Stanford University, Stanford, California.
24. Kneafsey, T., Blankenship, D., Dobson, P., White, M., Morris, J. P., Fu, P., Schwering, P. C., Ajo-Franklin, J. B., Huang, L., Knox, H. A., Strickland, C., Burghardt, J., Johnson, T., Neupane, G., Weers, J., Horne, R., Roggenthen, W., Doe, T., Mattson, E., & EGS Collab Team. (2021a). *The EGS Collab Project: Status and Accomplishments*. Paper presented at the 2021 Geothermal Rising Conference, GRC Transactions, Vol. 45, 2021.
25. Kneafsey, T., Blankenship, D., Dobson, P., White, M., Morris, J. P., Fu, P., Wu, H., Schwering, P. C., Ajo-Franklin, J. B., Huang, L., Knox, H. A., Neupane, G., Weers, J., Horne, R., Roggenthen, W., Doe, T., & EGS Collab Team. (2021b). *Fracture Stimulation and Chilled-water Circulation Through Deep Crystalline Rock: Characterization, Modeling, Monitoring, and Heat-transfer Assessment*. Paper presented at the 46th Workshop on Geothermal Reservoir Engineering, Stanford University, Stanford, California.
26. Kneafsey, T. J., Dobson, P. F., Blankenship, D., Schwering, P. C., Morris, J. P., Fu, P., Wu, H., White, M. D., Knox, H. A., Ajo-Franklin, J. B., Huang, L., Neupane, G. H., Horne, R., Roggenthen, W., Weers, J., Doe, T. W., Mattson, E., & EGS Collab Team. (2021c). *Field Experiments and Model Validation: the EGS Collab Project*. Paper presented at the 55th U.S. Rock Mechanics/Geomechanics Symposium.
27. Kneafsey, T. J., Dobson, P. F., Ulrich, C., Hopp, C., Rodríguez-Tribaldos, V., Guglielmi, Y., Blankenship, D., Schwering, P. C., M., I., Burghardt, J. A., White, M. D., Johnson, T. C., Strickland, C., Vermuel, V., Knox, H. A., Morris, J. P., Fu, P., Smith, M., Wu, H., Ajo-Franklin, J. B., Huang, L., Neupane, G., Horne, R., Roggenthen, W., Weers, J., Doe, T. W., & EGS Collab Team. (2022c). *The EGS Collab Project – Stimulations at Two Depths*. Paper presented at the 56th US Rock Mechanics/Geomechanics Symposium, Santa Fe, New Mexico, USA.
28. Mattson, E., Neupane, G., Hawkins, A., Burghardt, J., Ingraham, M., Plummer, M., & EGS Collab Team. (2019a). Fracture Tracer Injection Response to Pressure Perturbations at an Injection Well. *GRC Transactions, 43*.
29. Mattson, E., Plummer, M., Neupane, H., Vermeul, V., Sirota, D., Ingraham, M., Kneafsey, T., & Team, T. E. C. (2023). *Fluorescein Tracer Testing on the 4100L – A Preliminary Examination of Initial Arrival in Wells and the Drift at the Second EGS Collab Testbed*. Paper presented at the 48th Workshop on Geothermal Reservoir Engineering, Stanford University, Stanford, California.
30. Mattson, E., Zhang, Y., Hawkins, A., Johnson, T., Ajo-Franklin, J., Neupane, G., & EGS Collab Team. (2019b). *Preliminary Collab Fracture Characterization Results from Flow and Tracer Testing Efforts* Paper presented at the 44th Workshop on Geothermal Reservoir Engineering, Stanford University, Stanford, California.

31. Meng, M., Frash, L. P., Carey, J. W., Welch, N. J., Li, W., & Peterson, S. K. (2021a). *Triaxial Direct-shear Reveals the True Magnitude of Shear Fracture Roughness Effects on Flow*. Paper presented at the SPE/AAPG/SEG Unconventional Resources Technology Conference.
32. Meng, M., Frash, L. P., Li, W., Welch, N. J., & Carey, J. W. (2021b). *Measurement of Geomechanical and Hydrological Properties of EGS-Collab Geothermal Rocks*. Paper presented at the 55th US Rock Mechanics/Geomechanics Symposium, Houston, Texas, USA.
33. Meng, M., Frash, L. P., Li, W., Welch, N. J., Carey, J. W., Morris, J., Neupane, G., Ulrich, C., & Kneafsey, T. (2022). Hydro-Mechanical Measurements of Sheared Crystalline Rock Fractures With Applications for EGS Collab Experiments 1 and 2. *Journal of Geophysical Research: Solid Earth, 127*(2), e2021JB023000. doi:https://doi.org/10.1029/2021JB023000
34. Morris, J. P., Dobson, P., Knox, H., Ajo-Franklin, J., White, M. D., Fu, P., Burghardt, J., Kneafsey, T. J., Blankenship, D., & EGS Collab Team. (2018). *Experimental Design for Hydrofracturing and Fluid Flow at the DOE Collab Testbed*. Paper presented at the 43rd Workshop on Geothermal Reservoir Engineering, Stanford University, Stanford, California.
35. Neupane, G., Mattson, E. D., Plummer, M. A., & EGS Collab Team. (2020). *Results of Multiple Tracer Injections into Fractures in the EGS Collab Testbed-1*. Paper presented at the 45th Workshop on Geothermal Reservoir Engineering, Stanford University, Stanford, California.
36. Oldenburg, C., Dobson, P., Wu, Y., Cook, P., Kneafsey, T., Nakagawa, S., Ulrich, C., Siler, D., Guglielmi, Y., Ajo-Franklin, J., Rutqvist, J., Daley, T., Birkholzer, J., Wang, H. F., Lord, N. E., Haimson, B. C., Sone, H., Vigiliante, P., Roggenthen, W. M., Doe, T. W., Lee, M. Y., Ingraham, M., Huang, H., Mattson, E. D., Zhou, J., Johnson, T. J., Zoback, M. D., Morris, J. P., White, J. A., Johnson, P. A., Coblentz, D. D., & Heise, J. (2020, 2020-11-23). *Hydraulic fracturing experiments at 1500 m depth in a deep mine: Highlights from the kISMET project*, United States.
37. Roggenthen, W., & King, D. (2017). *Quick Review of T data for kISMET Area (5/19/17)*. Retrieved from
38. Schwering, P., Ingraham, M., Vermeul, V., Burghardt, J., Johnson, T., Strickland, C., White, M., Hopp, C., Tribaldos, V. R., Kneafsey, T., Artz, T., Mattson, E., Doe, T., & Team, T. E. C. (2023). *Shut-In Testing on the 4100L - Implications on the State of Stress, Fractures, and Wellbores in the Second EGS Collab Testbed*. Paper presented at the 48th Workshop on Geothermal Reservoir Engineering, Stanford University, Stanford, California.
39. Singh, A., Zoback, M., Dobson, P. F., Kneafsey, T. J., Schoenball, M., Guglielmi, Y., Ulrich, C., Roggenthen, W., Uzunlar, N., Morris, J., Fu, P., Schwering, P. C., Knox, H. A., Frash, L., Doe, T. W., Wang, H., Condon, K., Johnston, B., & EGS Collab Team. (2019). Slip tendency analysis of fracture networks to determine suitability of candidate testbeds for the EGS Collab hydroshear experiment. *Geothermal Resources Council Transactions, 43*, 405–424.
40. Ulrich, C., Dobson, P. F., Kneafsey, T. J., Roggenthen, W. M., Uzunlar, N., Doe, T. W., Neupane, G., Podgorney, R., Schwering, P., Frash, L., Singh, A., & EGS Collab Team. (2018). *The Distribution, Orientation, and Characteristics of Natural Fractures for Experiment 1 of the EGS Collab Project, Sanford Underground Research Facility*. Paper presented at the 52nd U.S. Rock Mechanics/Geomechanics Symposium, Seattle, Washington.
41. White, M., Johnson, T., Kneafsey, T., Blankenship, D., Fu, P., Wu, H., Ghassemi, A., Lu, J., Huang, H., Neupane, G., Oldenburg, C., Doughty, C., Johnston, B., Winterfeld, P., Pollyea, R., Jayne, R., Hawkins, A., Zhang, Y., & EGS Collab Team. (2019). *The Necessity for Iteration in the Application of Numerical Simulation to EGS: Examples from the EGS Collab Test Bed 1*. Paper presented at the 44th Workshop on Geothermal Reservoir Engineering, Stanford University, Stanford, California.
42. White, M. D., Fu, P., Ghassemi, A., Huang, H., Rutqvist, J., Johnston, B., & EGS Collab Team. (2018). *Numerical Simulation Applications in the Design of EGS Collab Experiment 1*. Paper presented at the 43rd Workshop on Geothermal Reservoir Engineering, Stanford University, Stanford, California.
43. Williams, C. F., Reed, M. J., Mariner, R. H., DeAngelo, J., & Galanis Jr., S. P. (2008). *Assessment of moderate- and high-temperature geothermal resources of the United States*. (United States Geological Survey Fact Sheet 2008–3082). Retrieved from http://pubs.usgs.gov/fs/2008/3082/
44. Wu, H., Fu, P., Morris, J. P., Mattson, E. D., Hawkins, A. J., Zhang, Y., Settgast, R. R., Ryerson, F. J., & EGS Collab Team. (2019a). *Characterizing Fracture Flow in EGS Collab Experiment Based on Stochastic Modeling of Tracer Recovery*. Paper presented at the 44th Workshop on Geothermal Reservoir Engineering, Stanford University, Stanford, California.
45. Wu, H., Fu, P., Morris, J. P., Settgast, R. R., Ryerson, F. J., Mattson, E. D., Hawkins, A. J., & Zhang, Y. (2019b). *Stochastic modeling of a conservative tracer test for the characterization of fracture flow patterns in EGS Collab Experiment 1*. Paper presented at the 53rd US Rock Mechanics/Geomechanics Symposium, New York, NY, USA.
46. Zhang, Y., Dekas, A. E., Hawkins, A. J., Parada, A. E., Gorbatenko, O., Li, K., & Horne, R. N. (2020). Microbial Community Composition in Deep-Subsurface Reservoir Fluids Reveals Natural Interwell Connectivity. *Water Resources Research, 56*(2), e2019WR025916. doi:https://doi.org/10.1029/2019WR025916